Manuscript
Click here to download Manuscript: BOUN-D-15-00071_PK_rev_fv.docx
Click here to view linked References

Linkages between Boundary-Layer Structure and the Development of Nocturnal Low-Level Jets in Central Oklahoma

Petra M. Klein • Xiao-Ming Hu • Alan Shapiro • Ming Xue

Received: 17 May 2015, Revised: 01 September 2015

Abstract: In the Southern Great Plains, nocturnal low-level jets (LLJs) develop frequently after sunset and play an important role in the transport and dispersion of moisture and atmospheric pollutants. However, our knowledge regarding the LLJ evolution and its feedback on the structure of the nocturnal boundary layer (NBL) is still limited. In the present study, NBL characteristics and their interdependencies with the LLJ evolution are investigated using data sets collected across the Oklahoma City metropolitan area during the Joint Urban field experiment in July 2003 and from three-dimensional simulations with the Weather Research and Forecasting (WRF) model. The strength of the LLJs and turbulent mixing in the NBL both increase with the geostrophic forcing. During the nights with the strongest LLJs, turbulent mixing persisted after sunset in the NBL and a strong surface temperature inversion did not develop. However, the strongest increase in LLJ speed relative to the mixed layer wind speed in the daytime convective boundary layer (CBL) occurred when the geostrophic forcing was relatively weak and thermally induced turbulence in the CBL was strong. Under these conditions, turbulent mixing at night was typically much weaker and a strong surface-based inversion developed. Sensitivity tests with the WRF model confirm that weakening of turbulent mixing during the decay of the CBL in the early evening transition is critical for LLJ formation. The cessation of thermally induced CBL turbulence during the early evening transition triggers an inertial oscillation, which contributes to the LLJ formation.

Petra Klein, Xiao-Ming Hu, Alan Shapiro, Ming Xue.
School of Meteorology and Center for Analysis and Prediction of Storms, University of Oklahoma,
120 David L. Boren Blvd., Norman, Oklahoma, 73072, USA, email: pkklein@ou.edu and xhu@ou.edu

Keywords: Low-level jet · Nocturnal boundary layer · Stable boundary layer

1. Introduction

While much progress has been made in understanding the daytime convective boundary layer (CBL), our understanding regarding the night-time boundary layer has progressed more slowly and many challenges remain (Belusic and Guttler 2010, Mahrt 2007, 2009, 2011, 2014, Fernando and Weil 2010, Lareau et al. 2013, Banta et al. 2003, 2006, 2013, Holtslag et al. 2013, Bosveld et al. 2014). Under clear skies, turbulence in the CBL is predominantly generated near the surface due to solar heating of the ground and is then transported upward throughout the CBL by updrafts and downdrafts that have turnover times on the order of tens of minutes and length scales of up to 2-3 km. In contrast, in the nocturnal boundary layer (NBL) an inversion layer forms near the surface under clear-sky conditions, in which thermal effects suppress the generation of turbulence by wind shear. Thus, turbulent mixing within the atmospheric boundary layer rapidly declines during the early-evening transition, and may become weak and intermittent during very stable conditions (Acevedo and Fitzjarrald 2001, Mahrt 2010). The drastic drop in turbulent mixing during the early-evening transition is a key mechanism (Blackadar 1957, Shapiro and Fedorovich 2010) causing the formation of nocturnal low-level jets (LLJs). In the presence of LLJs, strong wind shear can sustain turbulent mixing and turbulence may be transported from aloft down to the surface (Smedman et al. 1997, Lundquist and Mirocha 2008, Hu et al. 2013b, Mahrt 1999, Ha and Mahrt 2001, Mahrt and Vickers 2002).

In the United States, LLJs are mostly documented and studied over the Great Plains (e.g., Bonner 1968, Mitchell et al. 1995, Stensrud 1996, Pan et al. 2004, Song et al. 2005, Jiang et al. 2007, Pu and Dickinson 2014, Duarte et al. 2012) and the eastern coastal area (Zhang et al. 2006, Helmis et al. 2013). The jet maximum (thereafter called LLJ nose) typically develops at altitudes ranging from few tens of metres to several hundreds of metres (Cuxart and Jiménez 2007, Zhang et al. 2006, Banta 2008, Werth et al. 2011, Wei et al. 2013). Several factors have been discussed

as leading to the formation of these nocturnal LLJs, including inertial oscillations (Blackadar 1957, Shapiro and Fedorovich 2010, Parish and Oolman 2010, van de Wiel et al. 2010, Shibuya et al. 2014), baroclinicity generated by sloping terrain (Holton 1967), conservation of potential vorticity (PV) (Zhong et al. 1996), and large-scale meteorological forcing (Song et al. 2005, Wei et al. 2013, Hu et al. 2013b). However, the inertial oscillation theory appears incomplete as it cannot explain the geographical preference of LLJs and does not match well with observed LLJ characteristics (Shapiro and Fedorovich 2009, Lundquist 2003). The terrain-associated baroclinicity theory (Holton 1967) cannot correctly reproduce the jet-like vertical profiles (Shapiro and Fedorovich 2009). In the PV conservation theory, northward-moving airflow becomes jet-like horizontally, as the Coriolis parameter increases with increasing latitude (Wexler 1961). However, this theory cannot explain the diurnal cycle of LLJs and their jet-like shape in the vertical. The development of LLJs may also be modulated by atmospheric radiative cooling (Holton 1967, Baas et al. 2009, Edwards et al. 2014) or, more generally, the surface energy balance (Fast and Mccorcle 1990). Thus, the dynamical origin of nocturnal LLJs is still controversial and studies are still being conducted to extend/complete the previous theories (e.g., Shapiro and Fedorovich 2009, van de Wiel et al. 2010).

Different theories regarding the LLJs formation also have implications for vertical profiles of turbulence and other related meteorological and chemical variables (Kutsher et al. 2012). The time evolution and vertical distribution of mean and turbulent properties in the NBL are still active topics of research (Banta et al. 2006, Banta 2008, Ohya et al. 2008, van de Wiel et al. 2012a, Hu et al. 2013a,d, Chambers et al. 2011, Karipot et al. 2008). Turbulent mixing in the NBL intensifies for wind speeds above a critical value (Sun et al. 2012, Bonin et al. 2015). For low wind speeds, the stable layer adjacent to the surface typically decouples from the residual layer, and the decay of mixing after the early-evening transition causes sharp gradients in wind and temperature profiles near the surface. For higher wind speeds, stronger vertical mixing prevails near the surface and also between the surface and residual layer, i.e. these layers stay coupled (Acevedo et al. 2012, Hu et al. 2012). The impact of vertical mixing associated with LLJs on the vertical

92 distribution of meteorological variables and chemical species needs to be further
93 investigated (Banta et al. 2002, Cuxart and Jiménez 2007, Hu et al. 2012, 2013a,d,
94 Williams et al. 2013).
95 In summary, open questions remain about the LLJ evolution and LLJ
96 interaction with the dynamic, thermodynamic, and turbulence structure of the NBL.
97 In part, this is due to the lack of high-resolution profile measurements that range
98 from the surface up to a few hundred metres above the LLJ nose (Conangla and
99 Cuxart 2006, Deppe et al. 2013, Banta et al. 2013, Helmis et al. 2013, Klein et al.
100 2015, Mahrt et al. 2014, Pichugina and Banta 2010, Wei et al. 2014, Duarte et al.
101 2012). In the present manuscript, linkages between characteristics of nocturnal
102 LLJs and the structure of the atmospheric boundary layer before and after sunset
103 are investigated. The analyses primarily use data sets collected during the Joint
104 Urban field experiment in July 2003 (JU2003) in Oklahoma City. This data set was
105 selected as it provides detailed radar wind profile measurements and turbulence
106 quantities measured on an 80-m tower. Data from the Oklahoma Mesonet provide
107 further information about near-surface winds and stability in the rural areas
108 surrounding Oklahoma City, which was shown to be correlated with LLJ
109 characteristics (Hu et al. 2013b). Previous analyses of the JU2003 data sets have
110 demonstrated that LLJs occurred on approximately 85% of the nights during the
111 JU2003 study period (Lundquist and Mirocha 2008). Wang et al. (2007) concluded
112 that the urban structures over downtown Oklahoma City lifted the LLJ nose by 25 -
113 100 m and reduced wind speeds below the LLJ nose by 10-15%, but direct transport
114 of turbulent momentum flux from the LLJ nose to the street level was not prominent.
115 DeWekker et al. (2004) compared temperature and wind profiles measured 2 km
116 upwind and 5 km downwind of the Oklahoma City central business district and
117 found that above 200 m differences in wind speed were less than 0.5 m s^{-1} and in
118 temperature less than 0.5 °C both during day and night. Thus, urban effects did
119 cause some changes in the LLJ characteristics but the urban impacts on the
120 dynamics of the LLJ and its development are generally minor and less prominent
121 than it was observed in other cities (Kallistratova et al. 2009). Our previous studies
122 using the JU2003 data focused on studying the differences in the thermodynamic

and turbulence structure of the NBL for nights with weak and strong LLJs and related impacts on the urban heat island intensity and nocturnal surface ozone concentrations (Hu et al. 2013b, Klein et al. 2014). The current study provides new insights about the scaling of mean flow and turbulence in the NBL and the mechanisms leading to LLJ development. In addition to the JU2003 data analysis, three-dimensional simulations with the Weather Research and Forecasting (WRF) model were conducted. Sensitivity tests with the WRF model reveal how the variation of turbulent friction affects LLJ development.

2. Method

2.1 Measurements

The JU2003 tracer experiment campaign took place in the Oklahoma City metropolitan area in July 2003 (Allwine et al. 2004). During this experiment, a boundary-layer radar wind profiler was operated almost continuously during the month of July 2003 in Oklahoma City at the Argonne National Laboratory (ANL) site, which was located 5 km downwind of the Oklahoma City central business district in a suburban area (Fig. 1b). The wind profiler collected data with a vertical resolution of 55 m and an average time interval of 25 min, providing coverage from 82 m to approximately 2700 m above ground level (a.g.l.) (De Wekker et al. 2004).

Mean and turbulent flow properties were measured with sonic anemometers at 37.3 m and 79.6 m a.g.l. at the Tyler Media (TM) tower (Fig. 1b). The TM tower was located 5.5 km south of the Oklahoma City central business district in suburban terrain (Grimmond et al. 2004). The mean wind speeds measured at these levels, referred to as U_{37} and U_{80} thereafter, are used to evaluate the NBL shear near the surface and U_{37} is also used as scaling velocity for turbulent quantities measured at the same height. Friction velocity u_*, defined as

$$u_* = \left[\left(\overline{u'w'}\right)^2 + \left(\overline{v'w'}\right)^2\right]^{1/4}, \quad (1)$$

and the turbulent velocity scale U_t computed according to

$$U_t = \sqrt{0.5(\sigma_u{}^2 + \sigma_v{}^2 + \sigma_w{}^2)} \quad (2)$$

152 are used to characterize the degree of turbulent mixing in the surface layer (see also
153 Sun et al. 2012). Turbulence kinetic energy, e, is equal to U_t^2. The turbulent
154 kinematic momentum fluxes $\overline{u'w'}$ and $\overline{v'w'}$ and standard deviations of the three
155 velocity components σ_u, σ_v, σ_w, are computed using the sonic-anemometer data
156 measured at the 37-m level. These data were originally processed using 30-min
157 averaging periods, but for the current analysis the 30-min statistics are further
158 averaged into hourly values.

159 Near-surface meteorological variables, including wind at 2 and 10 m a.g.l. and
160 air temperature at 1.5 and 9 m a.g.l., routinely collected at the Oklahoma Mesonet
161 sites, were also used in the analysis. (McPherson et al. 2007). The mean spacing
162 between Mesonet stations is approximately 30 km (Fiebrich and Crawford 2001).
163 The average 10 m wind speed at the six Mesonet sites around Oklahoma City (Fig.
164 1a,b) is calculated and analyzed as a measure of the near surface winds around
165 Oklahoma City. To investigate the influence of atmospheric stability in the surface
166 layer, the Richardson number (Ri) at the Mesonet sites is calculated as

167 $$Ri = \frac{g[(T_9 - T_{1.5})/\Delta z_T + \Gamma_d]\Delta z_u{}^2}{T_{1.5}[u_{10} - u_2]^2} \qquad (3)$$

168 where g is the acceleration due to gravity, the value adopted for the dry adiabatic
169 lapse rate Γ_d was $0.01°\text{C m}^{-1}$, T_9 and $T_{1.5}$ are the air temperatures measured at 9
170 and 1.5 m a.g.l., and u_2 and u_{10} are the wind speeds at 2 and 10 m a.g.l., respectively.
171 The height differences between the measurement levels are $\Delta z_T = 7.5$ m for air
172 temperature and $\Delta z_u = 8.0$ m for wind speed.
173
174 2.2 Numerical simulations
175 To systematically investigate the relationship between LLJs and boundary
176 layer characteristics, numerical simulations with the WRF model, version 3.4.1
177 (Skamarock et al. 2008) were conducted for two contrasting episodes: strong LLJs
178 during July 7-9, and weak LLJs during July 17-19. Simulations covering 42 hours
179 were initialized at 0000 UTC[1] on 7, 8, 17, and 18, July, respectively. The first 18

[1] UTC = Central Standard Time (CST) + 6 h

hours of each simulation are treated as spin-up, and the remaining 24 hours (from 1200 CST on day 1 to 1100 CST on day 2) are analyzed. Five one-way nested domains (Fig. 1c) were employed, with horizontal grid spacings of 40.5, 13.5, 4.5, 1.5, and 0.5 km, respectively. This set-up was chosen because previous studies have shown that a 0.5-km grid spacing is needed to resolve urban effects on the boundary-layer structure over Oklahoma City (Liu et al. 2006, Lemonsu et al. 2009, Hu et al. 2013). Each domain had 48 vertical layers extending from the surface to 100 hPa. The model sigma levels and mid-layer heights of the lowest 20 model layers are shown in Table 1. In all model domains, the Dudhia shortwave radiation algorithm (Dudhia 1989), the Rapid Radiative Transfer Model for longwave radiation (Mlawer et al. 1997), the WRF single-moment six-class (WSM6) microphysics scheme (Hong et al. 2004), and the Noah land surface scheme coupled with a single-layer urban canopy model (Chen et al. 2011) were used. Our study focuses on days during which clouds and precipitation did not develop over the study area. The microphysics scheme is thus only of relevance for resolving cloud processes in the outer domains, which cover significant portions of North America and where clouds were present during the study period.

Planetary boundary layer (PBL) schemes are used to parameterize turbulent vertical mixing of variables. The choice of PBL scheme affects the structure of the simulated boundary layers and how much vertical mixing is predicted, which leads to differences in the predicted LLJs strength (Nielsen-Gammon et al. 2010, Shin and Hong 2011, Draxl et al. 2014, Storm et al. 2009, Hu et al. 2013a). In order to investigate the impact of the boundary layer characteristics on LLJ formation, a sensitivity analysis is conducted for the Yonsei University (YSU, Hong et al. 2006, Hong 2010) PBL scheme. The YSU scheme is a first-order nonlocal scheme, with a counter-gradient term and an explicit entrainment term in the turbulence diffusion equation, which was shown to reproduce important features of the NBL (Hu et al. 2013a,c). In the YSU PBL scheme, the momentum eddy diffusivity for the stable boundary layer is formulated as

$$K_m = k w_s z (1 - \frac{z}{h})^2, \quad (4)$$

where the velocity scale is $w_s = u_*/\phi_m$, k is the von Karman constant, z is the height above ground, and h is the boundary layer height diagnosed in the YSU scheme using a critical Richardson number (0.25 over the land, while it depends on the surface winds and Rossby number over oceans). The non-dimensional profile function, ϕ_m, for stable conditions ($z/L > 0$) in YSU is implemented as

$$\phi_m = 1 + a\frac{z}{L}, \quad (5)$$

where L is the Monin-Obukhov length. The coefficient a, which describes the dependence of eddy diffusivity on the stability parameter z/L, plays an important role for simulating LLJs. Its default value in YSU is 5 (Nielsen-Gammon et al. 2010, Hu et al. 2013a). Sensitivity simulations with a varying between 0.1 and 10 are conducted. Note that the lower and higher values of this range may exceed the plausible range of a to accurately simulate the realistic vertical mixing in the nocturnal boundary layer (Foken 2006, Nielsen-Gammon et al. 2010). These extreme, somewhat unrealistic values were included to emphasize the role of stability and vertical mixing in LLJ development. In the standard WRF model output, available for all the conducted sensitivity simulations, only the eddy diffusivity for heat defined as

$$K_h = Pr^{-1}K_m, \quad (6)$$

where Pr is the turbulent Prandtl number, was saved. We thus used K_h to characterize the diurnal evolution of vertical turbulent mixing in the boundary layer, but verified for the control simulation (with $a = 5$) that the eddy-diffusivity profiles for heat and momentum are similar.

3. Results

3.1 Observed LLJ Properties

During July 2003, southerly winds dominated and LLJs developed in Oklahoma on a majority of the nights (Figs. 2a,b). Notable exceptions were July 1, when an easterly wind persisted due to a tropical depression east of Oklahoma, and July 22-23, 29-30, and the later half of July 10, when northerly winds dominated due to cold frontal passages. On one to two nights after each cold frontal passage, the LLJs were

typically relatively weak. In July 2003, the LLJ nose was typically at about 400 m and never above 800 m (Figs. 2a, 3). Following Hu et al. (2013b), the maximum jet speed, U_{LLJ}, was thus determined as the hourly maximum wind speed observed in the layer between 200 - 800 m. The lower limit of 200 m was chosen, as the radar wind profile data may not be accurate below these heights.

The Richardson number Ri (3) shows distinct diurnal patterns around Oklahoma City during the study period (Fig. 2c). It increases prominently during the early evening transition and remains positive until the next morning when the rapidly developing convective boundary layer breaks down the near-surface inversion. As, the day-to-day variation of Ri is prominent, one objective of our study is to investigate the relationships between atmospheric stability and LLJ strength. We selected a 12-h time period for each day/night ranging from 1730 to 0430 local time (LT which during the study period is equal to CDT). The analyzed data were limited to days/nights for which the wind directions measured at the Tyler Media tower at 37-m and 80-m a.g.l. were within a southerly sector (135^{o}-225^{o}), and for which the observations had no major gaps during the selected 12-hr windows. The time period was chosen to study the transitions from the afternoon CBL to the stable NBL. The sunset times, which ranged from 2049 – 2035 LT in July 2003, were taken into account when defining the time window. Table 2 lists the 18 days in July 2003 included in the analysis and provides an overview of important boundary layer parameters, which are defined and discussed below. Each listed date refers to the day at the beginning of the time window. The sonic anemometer at the 37-m level became fully operational only on July 06, which is why some of the data are missing for the first 3 days. Daytime and nighttime wind profiles for the selected nights are shown in Fig. 3a-c. The daytime profile was computed as the average of the 1730 and 1830 LT observations, for the nighttime profile three hourly profiles from 0130 – 0330 LT were averaged since the properties of the LLJ for most days did not vary much in that time period. The profiles show that the daytime values of U_{LLJ}, computed as maximum wind speed below 800 m, are representative of the mixed layer wind speeds in the daytime CBL while at night U_{LLJ} corresponds to the LLJ wind speed maximum.

The daily time series of the wind speeds U_{LLJ}, U_{37}, and U_{80}, friction velocity u_*, turbulent velocity scale U_t , and Richardson number *Ri* for the 18 selected days are shown in Fig. 4. The transition from unstable conditions (*Ri*<0) to stable conditions (*Ri*>0) happens at around 2000 LT (Fig. 3f). Around that time, U_{LLJ} begins to increase until it starts to level off at around 0100 during most nights. On seven days, U_{LLJ} drops at around 1930 LT (most pronounced on July 03 and July 26) before the winds start to accelerate. van de Wiel et al. (2010) discuss that backward inertial oscillations can initially cause a drop in wind speed but such backward oscillations should occur below a crossing point near the surface. For the current paper, we focused on analyzing correlations between bulk LLJ and turbulence characteristics and did not further investigate if backward oscillations may have caused the observed initial drops in wind speed.

During the 18 nights analyzed, the maximum LLJ speed $\left(U_{LLJ}\right)_{max}$ observed each night varied between 14.4 m s^{-1} and 22.5 m s^{-1} (Table 2) while the shape of the daily time series of U_{LLJ} is quite similar (Fig. 4). Following the inertial oscillation theory, the LLJ speed depends on the deviation of the boundary layer winds from the geostrophic wind, i.e. the ageostrophic wind speed (Shapiro and Fedorovich 2010, van de Wiel et al. 2010). Getting reliable estimates of the geostrophic wind speed proved to be challenging, i.e. we could not compute the ageostrophic wind speed that was proposed as scaling velocity in the literature (Shapiro and Fedorovich 2010, van de Wiel et al. 2010). Above 800 m, the daytime wind speed profiles (average of the profiles measured at 1730-1830 LT) show little variability with height, i.e. the daytime values of U_{LLJ} are a good approximation of the mixed layer wind speed in the CBL (Figs. 3a-c). Thus, we decided to define the daytime values of U_{LLJ}, as a scaling velocity U_s. While we expect the geostrophic wind speed to be higher than U_s, we hypothesize that this scaling velocity can serve as a proxy which allows us to account for the variability in the geostrophic forcing. The values of U_s ranged from 6.5 to 10.9 m s^{-1} during the study period (Table 2). Normalized daytime and nighttime profiles using U_s as scaling velocity are shown in Fig. 3d-f. It can be noted that days with the highest velocity increase at night, i.e. days with the

highest U_{LLJ}/U_s values, are not the days with the highest values of U_{LLJ}. While the normalized profiles show less variability than the original wind profiles, the relative low-level jet strength and height still vary from day to day. Finding the factors causing this variability is an important objective of this study.

The trends in the time series of U_{37}, and U_{80} are less consistent (Fig. 4b, c) than the trends in U_{LLJ}, and also the friction velocities u_* vary strongly (Fig. 4d) whereby large differences are particularly noticeable before sunset: on some days a pronounced increase in u_* is observed before the early-evening transition while on other days a gradual decline or high variability from hour to hour can be noted. The turbulent velocity scale U_t, on the other hand, shows similar trends for all days and more consistent trends throughout the selected 12-hour time window. Thus, U_t is used as a parameter to describe the level of turbulent mixing in the NBL, which is also consistent with the study of Sun et al. (2012). The *Ri* profiles have similar shapes but both the afternoon values Ri_{day} (minimum *Ri* value before sunset) and nighttime value Ri_{night} (maximum *Ri* value observed between 2230 and 0430 LT) vary daily during the study period (Fig. 3f). The values Ri_{night} ranged from 0.03 to 0.25, i.e. from quasi-neutral to moderately stable conditions, for Ri_{day} values in the range of -0.07 to -0.38 were observed (Table 2).

As discussed in Shapiro and Fedorovich (2010) and van de Wiel et al. (2010), the LLJ starts to develop as an inertial oscillation from the initial afternoon wind profile and the increase in wind speed relative to the initial wind speed is an important parameter that describes the LLJ strength. In our analysis, the wind speed ratio U_{LLJ}/U_s describes the increase of the wind speed at the LLJ nose relative to the initial mixed-layer wind speed. The diurnal time series of U_{LLJ}/U_s (Fig. 5a) show the expected sharp increase of U_{LLJ}/U_s after the early-evening transition. The variation of U_{LLJ}/U_s with *Ri*-number further highlights the sharp increase as stability changes from unstable to stable conditions. However, the U_{LLJ}/U_s-values start to decline again for $Ri > 0.1$ and a clear correlation between the *Ri* values at night ($Ri > 0.1$) and U_{LLJ}/U_s does not emerge (Fig. 5d). The daily maximum ratios $\left(U_{LLJ}/U_s\right)_{max}$ ranged between 1.8 and 2.7 (Table 2). As additional parameters describing the

dynamic and turbulent structure of the NBL, the velocity ratio U_{80}/U_{37}, and turbulent velocity scale U_t/U_{37} normalized by the wind speed measured at the same height and time are also plotted in Fig. 5. The ratio U_{80}/U_{37} can serve as a dimensionless shear parameter, since

$$\frac{U_{80}}{U_{37}} = \frac{80-37}{U_{37}}\frac{dU}{dz} + 1 \qquad (7),$$

which describes the degree of shear below the LLJ nose. The ratio U_t/U_{37} is a measure of the turbulence intensity. The variation of U_t/U_{37} with stability is more consistent than for U_{LLJ}/U_s: turbulence intensity decreases nearly linearly as *Ri* increases (Fig. 5.f). Similar to U_{LLJ}/U_s, the shear parameter U_{80}/U_{37} increases drastically after *Ri* becomes positive, but a clear correlation between *Ri* and U_{80}/U_{37} does not emerge (Fig. 5.f). It is interesting to note that high values of $\left(U_{LLJ}/U_s\right)_{max}$, i.e. the development of a strong LLJ relative to the previous day mixed-layer wind speed, appear to be more prominent on days with lower Ri_{day} values, such as e.g. on July 18, 26, and 27 (Table 2 and Fig. 5d). During these three days, the highest turbulence intensities U_t/U_{37} (Fig. 5b, e) were observed in the CBL. The correlation between relative LLJ strength $\left(U_{LLJ}/U_s\right)_{max}$, and atmospheric stability *Ri* and turbulence intensity U_t/U_{37} at different times is now investigated in more detail.

Following the inertial oscillation theory, the drop in turbulent vertical mixing during the early-evening transition determines the strength of the LLJ relative to the initial (afternoon mixed-layer) wind speeds (Shapiro and Fedorovich 2010, van de Wiel et al. 2010). Thus, we propose the hypothesis that the highest increase of the LLJ speed relative to the initial mixed-layer wind speed, i.e. the highest value of $\left(U_{LLJ}/U_s\right)_{max}$, is expected during nights with (i) the largest change in atmospheric stability, i.e. largest values of $Ri_{night} - Ri_{day}$ and (ii) the strongest drop in turbulence intensity U_t/U_{37} during the early-evening transition. During the study period, the change in atmospheric stability, $Ri_{night} - Ri_{day}$, varied from 0.13 on July 06 to 0.57 on July 18. To assess the change in turbulence intensity, we computed a daytime value $(U_t/U_{37})_{day}$ as a mean value for the time period 1730-1830 LT, and nighttime value $(U_t/U_{37})_{night}$ as the minimum value observed

between 2230 and 430 LT (Table 2). During the study period, the ratio $(U_t/U_{37})_{night}/(U_t/U_{37})_{day}$, which describes the drop in turbulence intensity from the daytime CBL to the NBL values, ranged between 0.33 on July 18 and 0.91 on July 07.

Plots of the relative LLJ strength $\left(U_{LLJ}/U_s\right)_{max}$ versus the change in stability $Ri_{night} - Ri_{day}$ (Fig 6a), and the drop in turbulence intensity $(U_t/U_{37})_{night}/(U_t/U_{37})_{day}$ (Fig. 6d) show the expected trends: $\left(U_{LLJ}/U_s\right)_{max}$ increases as the change in stability $Ri_{night} - Ri_{day}$ increases and as the ratio of nighttime to daytime turbulence intensity $(U_t/U_{37})_{night}/(U_t/U_{37})_{day}$ decreases. The scatter in the data is however fairly large and the correlation coefficients r are quite low (0.41 and 0.3 respectively). In addition to relative LLJ strength, the shear parameters U_{80}/U_{37} and U_{LLJ}/U_{37} are also plotted in Fig. 6. As one would expect, both shear parameters also increase with increasing $Ri_{night} - Ri_{day}$ and decrease with increasing $(U_t/U_{37})_{night}/(U_t/U_{37})_{day}$. The corresponding correlation coefficients are quite high, particularly for U_{80}/U_{37} and $(U_t/U_{37})_{night}/(U_t/U_{37})_{day}$, as in that case all variables were measured at the same site and with the same instruments.

As mentioned above, the relative LLJ strength $\left(U_{LLJ}/U_s\right)_{max}$ tended to be higher on days with lower (characterizing more convective conditions) Ri numbers before the early-evening transition. We thus also investigated correlations of the relative LLJ strength and shear parameters with values of daytime and nighttime stability (Ri_{day} and Ri_{night}) and turbulence intensity $\left[(U_t/U_{37})_{day}\right.$ and $\left.(U_t/U_{37})_{night}\right]$. Of all six parameters represented in Fig. 6, relative LLJ strength $\left(U_{LLJ}/U_s\right)_{max}$ correlates best with Ri_{day} (Fig. 6b) and shows no correlation with the nighttime stability Ri_{night} (Fig. 6c) or turbulence intensity $(U_t/U_{37})_{night}$ (Fig. 6f). The shear parameters, on the other hand, are best correlated with $(U_t/U_{37})_{night}$ (Fig. 6f). It thus appears that in our study, relative LLJ strength primarily depends on daytime stability and turbulence intensity but is not noticeably affected by the nighttime stability. One interpretation is that the collapse of the CBL during the early-evening transition is the main mechanisms triggering

389 the initial LLJ development. The LLJ then persists throughout the night with its bulk
390 characteristics not being much affected by nighttime stability and turbulence
391 intensity. The latter two parameters do however modulate the shear below the LLJ
392 nose. At the same time, nighttime stability and turbulence parameters are also
393 modulated by the presence of the LLJ at night. As a consequence, the values of
394 $(U_t/U_{37})_{night}$ do not vary much throughout the study period, i.e. daily variations in
395 the turbulence intensity ratios $(U_t/U_{37})_{night}/(U_t/U_{37})_{day}$ are primarily due to
396 variations in the daytime values. Our findings overall confirm the hypotheses that
397 were formulated above based on the inertial oscillation theory: the relative LLJ
398 strength depends on the degree of change in atmospheric stability and turbulence
399 intensity during the early-evening transition. Additionally, we have shown that the
400 conditions in the daytime CBL just before sunset are critical and the daytime Ri_{day} is
401 a good indicator for the strength of LLJ. These conclusions may not be applicable to
402 situations with weaker jets and strongly stable NBLs.
403 Our analysis so far, has followed the concepts outlined in Shapiro and
404 Fedorovich (2010) and van de Wiel et al. (2010) and conclusions we derived have
405 been based on the relative LLJ strength, i.e. the increase in velocity relative to the
406 mixed-layer velocity prior to the early-evening transition. We would like to point
407 out that such normalization by an initial wind speed is critical. As shown in Fig. 7,
408 very different conclusions could be drawn if the absolute wind speed U_{LLJ} is plotted
409 against atmospheric stability. The daily maximum values of U_{LLJ} correlate well with
410 all 3 stability parameters $Ri_{night} - Ri_{day}$, Ri_{night}, and Ri_{day} but LLJ strength
411 increases as the absolute values of *Ri* decrease, i.e. when the flow becomes more
412 neutral. One may thus conclude that stability effects play no important role in the
413 LLJ development and that the LLJ weakens as the daytime CBL becomes more
414 unstable and the NBL more stable. However, the fact that stronger LLJs correspond
415 with more neutral conditions merely reflects the fact that atmospheric stability, in
416 general, decreases as wind speed increases. As illustrated in Fig. 7, the same trends
417 are observed for the average wind speeds measured at the six rural Mesonet sites
418 10 m above ground (U_{10}) and for the wind speeds measured on the Tyler Media

tower shown in Fig. 1b (U_{37} and U_{80}). Appropriate normalization of the data is thus key for understanding which factors play a role in the development and evolution of LLJs. In our study, using the daytime mixed-layer wind speed as a scaling velocity U_s allowed us to account for the general trends in the geostrophic forcing and to analyze the data in a non-dimensional framework.

Similarly, we want to point out the importance of using turbulence intensities U_t/U_{37} rather than original values of U_t when investigating the role of turbulent mixing in LLJ development. There are no big differences in the nighttime to daytime ratios of these two quantities (Figs. 6d and 7d), but opposite trends are observed in the correlation of relative LLJ strength $\left(U_{LLJ}/U_s\right)_{max}$ with daytime values: while we observe the expected trend of stronger daytime turbulence intensities $(U_t/U_{37})_{day}$ promoting stronger LLJs, higher absolute values of $U_{t,day}$ correlate with weaker LLJs. One explanation is that the decline of turbulent mixing during the early-evening transition, which drives the inertial oscillation, is primarily due to the shut down of thermally driven turbulence. The intensity of thermally driven turbulence in the CBL thus becomes a dominant factor leading to LLJ development. High values of $U_{t,day}$ can be observed during days with high wind speeds during which thermally driven turbulent mixing is of secondary importance. Thus, the magnitude of $U_{t,day}$ does not necessarily describe well the level of thermally driven turbulence and is apparently inadequate as parameter for LLJ development. On the other hand, the turbulence intensities, that describe the strength of turbulent mixing relative to the mean flow, are better indicators of thermally driven turbulence.

3.2 Analysis of Selected Episodes

The interdependence between boundary layer characteristics/structures and LLJs are further examined in detail for two contrasting episodes during July 7-9 and during July 17-19 (Fig. 8). During the July 7-9 episodes, the maximum LLJ wind speeds were higher than 21 m s^{-1}, while during the July 17-19 episodes the maximum LLJ wind speed stayed around 15 m s^{-1} (Table 2 and Fig. 4). So, in terms of absolute wind speeds, a weaker LLJ developed during the second episode. However,

449 the strongest increase relative to the daytime winds was observed during the night
450 of July 18-19. On July 18, daytime stability Ri_{day} was -0.37 while the CBL during the
451 first episode was less unstable ($Ri_{day} \approx -0.1$). Turbulence intensity in the daytime
452 CBL, $(U_t/U_{37})_{day}$, had the highest value on July 18 of all the days analyzed, which
453 further indicates that the contribution of thermally driven turbulent mixing in the
454 CBL was stronger during the second than the first episode. Synoptic flow patterns
455 played an important role in modulating the wind speeds for the two episodes.
456 During July 7-9, the pressure gradient over most of the Great Plains was northwest-
457 to-southeast. Such a synoptic-scale weather pattern predominates during the warm
458 season (Song et al. 2005). The horizontal pressure gradient and the blocking effect
459 of the Rockies (see terrain height in Fig. 1c) forced airflow from southerly latitudes
460 into the south-central United States, thus contributing to strong southerly or
461 southwesterly winds during the nighttime (Figs. 8a, 2b). During July 17-19, the
462 pressure gradient was weak in Oklahoma, resulting in weaker prevailing southerly
463 to southwesterly winds (Figs. 8b, 2b).

464 Weaker/stronger winds are associated with weaker/stronger turbulence
465 near the surface during the nighttime (Fig. 8a,b). Turbulence subsided quickly
466 during the early evening transitions of the episode of July 17-19 as indicated by a
467 sharp decrease of the turbulent velocity scale U_t and friction velocity (u_*). As
468 discussed above, the nighttime turbulence intensities dropped to roughly about 30%
469 of the daytime values on July 18. In contrast, the turbulent velocity scale
470 U_t remained relatively high throughout the nights of July 7-9 and on July 7 the
471 nighttime turbulence intensity was still approximately equal to 90% of the
472 corresponding daytime value (Table 2). The sharper drop in turbulence intensity
473 during the second episode was associated with a sharper increase in LLJ speed
474 relative to the daytime wind speeds, i.e. the values of $\left(U_{LLJ}/U_s\right)_{max}$ were higher
475 than during the first episode. Differences in the nighttime turbulence intensities also
476 were associated with clear differences in nighttime stability: higher wind speeds
477 and higher turbulence intensities at night were associated with stronger coupling in
478 the layer below the LLJ nose as indicated by the smaller values of the shear

parameter $(U_{80}/U_{37})_{max}$ (Tab. 2 and Fig 5b) and lower Ri_{night} values (Fig. 8c) during the first episode, while nighttime wind shear (Fig 5b) and stability quickly increased (Fig. 8d) due to surface radiative cooling in the absence of strong turbulence during the second episode. Differences can also be noted in the heights of the LLJ nose: during the second episodes the LLJ was lower than during the first episode. Our finding of nighttime turbulence increasing with large-scale pressure gradient forcing is consistent with van de Wiel et al. (2012b), who found that nighttime near-surface turbulence increased rapidly when the geostrophic wind exceeded 5 m s^{-1}.

3.3 WRF Simulations for the Selected Episodes

To further investigate the linkages of LLJ development and NBL structure, sensitivity studies were conducted with the WRF model in which the stability dependence of the eddy diffusivity was systematically varied. The control WRF simulations with default parameters successfully capture the differences in LLJ strength between the two episodes (Figs. 9a,b). On each day, turbulent vertical mixing (as characterized by the eddy diffusivity for heat K_h) in the boundary layer shows a prominent diurnal variation (Figs. 9c,d). Vertical mixing clearly weakens drastically after sunset, but while it becomes nearly negligible in the residual layer, some mixing persists in the stable boundary layer throughout the night (Figs. 9c,d).

The results from the WRF model sensitivity tests with different values for the coefficient a in the stability functions ϕ_m (Eq. 5) used in the YSU PBL scheme illustrate the feedback of boundary layer characteristics on LLJ development. In all simulations, the LLJ nose occurs near the top of the stable boundary layer (i.e. near the transition to the residual layer), where vertical mixing sharply declines (Figs. 10a,b) and the flow becomes effectively inviscid. Weak vertical mixing confined in a shallower stable boundary layer leads to lower LLJs (Figs. 10a-d). This is consistent with the observational study of Pichugina and Banta (2010), which reports that for a LLJ with a distinct nose, the height of the LLJ nose is approximately the height of the first significant minimum in the turbulence profile (or top of the stable boundary layer). Sharp contrasts in simulated nighttime stability during the two episodes also exist, which further documents how vertical mixing modulates boundary layer

stability (Figs 11e,f). During episode 1, when the geostrophic forcing, nocturnal LLJs, and vertical mixing at night were all strong, a nearly neutral boundary layer develops for all test scenarios (Fig. 10e) but the depth of this layer decreases as the mixing weakens. During episode 2, the control run (and also the runs with weaker mixing than in the control run) predicts a strong-surface based inversion, which weakens in the simulations with stronger mixing (Fig. 10f). The coincidence of the heights of LLJ nose and top of the stable boundary layer may be explained by the Blackadar's inertial oscillation theory: the oscillation amplitude is expected to grow as the ground is approached from the top of the residual layer until the frictional force inevitably becomes important near the surface in the stable boundary layer (Shapiro and Fedorovich 2010), i.e., the oscillation amplitude at night peaks at the top of the stable boundary layer (Blackadar 1957). The collocation of the LLJ nose and transition from the stable boundary layer to the residual layer also illustrates the importance of nearly zero mixing in the residual layer for the inertial oscillation. These results may also explain why lower LLJs (approximately 100m a.g.l.) are observed in shallower, stably-stratified ocean boundary layers (e.g., Smedman et al. 1995, Mahrt et al. 2014) than in the Southern Great Plains, where the LLJ mostly peaks above 200 m (Song et al. 2005).

Decreasing a in the YSU PBL scheme causes stronger vertical mixing that persists over a deeper layer, leading to higher and weaker LLJs (Fig. 10). Thus, the sensitivity study illustrates how vertical mixing tends to hamper the inertial oscillation and reduce LLJ strength. These results are consistent with the sensitivity tests using analytical models of nocturnal LLJs reported in Shapiro and Fedorovich (2010). In nearly all the quantitative studies of the inertial oscillation using analytical models, turbulent diffusivities or turbulent friction terms were prescribed as external forcings, thus neglecting feedback between the shear and turbulent mixing (Shaprio and Fedorovich 2009, 2010, van de Wiel et al. 2010, Schroter et al. 2013). This feedback, as shown above, can affect the eventual LLJ strength.

As discussed above, a sharp decrease of vertical mixing in the NBL (including both the stable boundary layer and the residual layer) during the early-evening transition can be noted during both episodes (Figs. 9c,d, Figs. 11c,f). The simulation

results provide additional evidence to the observations that the stronger dynamic forcing during episode 1 caused higher LLJ speeds U_{LLJ} (Fig. 11a) but weaker relative LLJ strength U_{LLJ}/U_s (Fig. 11b) than during episode 2 (Figs. 11 d,e). Time series (Figs. 11 c, f) of the peak values K_{hp} in the vertical eddy-diffusivity profiles show that the reduction in K_{hp} during the early-evening transition was larger during episode 2 (Fig. 11f) than during episode 1 (Fig. 11c). The fact that U_{LLJ}/U_s values were higher during episode 2 than during episode 1 confirms that a stronger reduction in vertical turbulent mixing leads to a stronger increase in wind speed after sunset. The results shown in Fig. 12 further illustrate that relative LLJ strength $\left(U_{LLJ}/U_s\right)_{night}$ (maximum value for each night) correlates well with the reduction of eddy diffusivity (expressed as the ratio K_{min}/K_{max} whereby K_{min} corresponds to the minimum value of K_{hp} observed at night and K_{max} to the maximum of K_{hp} before sunset). The results from both episodes and three different sensitivity tests all show a clear trend of increasing values in relative LLJ strength $\left(U_{LLJ}/U_s\right)_{night}$ as the drop in turbulent mixing during the early-evening transition becomes stronger, i.e. K_{min}/K_{max} decreases (Fig. 12a). No clear trends are observed when the actual LLJ speed $\left(U_{LLJ}\right)_{night}$ is plotted against K_{min}/K_{max} (Fig. 12b).

In summary, the sensitivity tests conducted with the WRF model have shown that (1) the numerical simulations are in qualitatively good agreement with observations, (2) the sharp drop in turbulent mixing during the early-evening transition triggers an inertial oscillation, which contributes to LLJ formation, and (3) the scaling of LLJ strength by a scaling velocity U_s is critical for investigating the factors leading to LLJ formation. The afternoon mixed layer wind speed, used in our study as scaling velocity U_s, overall works well but large differences can be noted between the observations and numerical model results for U_{LLJ}/U_s on the second day of episode 2 (Fig. 11e). The WRF model predicts much higher values for U_{LLJ}/U_s than what was observed. These differences can be explained by the underprediction of the afternoon mixed layer wind speed in the WRF output (Fig. 11d). As a result, the value of the scaling velocity U_s for the WRF model output was lower than for the

570 observations and consequently U_{LLJ}/U_s was overpredicted even though the
571 observed and simulated nighttime values of U_{LLJ} agreed well.
572
573 **4. Discussion and Conclusions**
574 The linkages between LLJ development and properties of the daytime CBL and
575 nighttime stable boundary layer have been investigated in this study by using
576 measurements collected in the Oklahoma City metropolitan area during the Joint
577 Urban 2003 field experiment, along with WRF simulations. Prominent LLJs
578 occurred on most nights during the JU2003 experiment. According to the inertial
579 oscillation theory (Blackadar 1957), nocturnal LLJs develop in response to the
580 collapse of turbulence in the CBL during the early-evening transition. Thus, nights
581 with strong temperature inversions and weak turbulence in a shallow, stable
582 boundary layer near the surface are often viewed as prone to the formation of
583 strong LLJs. Interestingly, the JU2003 dataset shows that stronger LLJs in central
584 Oklahoma in the summer time were always associated with stronger turbulence and
585 weaker inversions at night, which could be viewed as contradicting the Blackadar
586 (1957) theory. It is important, though, to find a framework for the data analysis,
587 which allows accounting for the influence of the geostrophic forcing. We have
588 shown that, in the absence of reliable data for the geostrophic winds, the mixed
589 layer wind speed of the daytime CBL can serve as an appropriate LLJ scaling velocity
590 U_s. Relative LLJ strength $\left(U_{LLJ}/U_s\right)_{max}$ correlates well with daytime Richardson
591 numbers Ri_{day} and turbulence intensities $(U_t/U_{37})_{day}$, while the corresponding
592 nighttime values of these two parameters primarily influence the shear below the
593 LLJ nose but do not correlate well with relative LLJ strength.
594 During nights with stronger LLJs, the wind speeds in the daytime CBL were
595 typically also higher, which indicates that during these days the geostrophic forcing
596 was stronger. As the geostrophic forcing becomes stronger, the rate of mechanically
597 generated turbulence increases both during day and night. It appears that if the
598 wind speed during the early-evening transition exceeds some critical value, vertical
599 mixing will persist throughout the night and a strong inversion will not develop

close to the surface. The development of nocturnal LLJs in absence of strong surface temperature inversions was also reported in some other regions (e.g., coastal area in high latitudes, Smedman et al. 1995, Helmis et al. 2013). However, even during nights with strong geostrophic forcing, a sharp drop in vertical mixing is still observed during the early-evening transition, which is sufficient to trigger an inertial oscillation. Three-dimensional modeling results further confirm that the sudden weakening of vertical mixing in the nocturnal boundary layer (including both the stable boundary layer and the residual layer) during the early evening transition contributes to LLJ formation. The level of mixing at night primarily modulates the thermodynamic structure of the NBL, the height of the LLJ nose and the shear below the jet nose. Stronger/weaker LLJs are associated with larger/smaller turbulence near the surface, which leads to weaker/stronger vertical gradients of temperature and wind speed. These results agree with previous studies (e.g., Lundquist and Mirocha 2008, Hu et al. 2013b, d), which also reported that strong LLJs coincide with strong turbulence near the surface, which modulates the NBL structure.

The NBL characteristics in the presence of LLJs have important implications for vertical dispersion and horizontal transport of heat, moisture and pollutants. Under the traditional view of the NBL, the mixing between the surface stable layer and the layer above is limited due to strong stratification. Thus, moisture and pollutants accumulated above the surface layer can be efficiently transported horizontally overnight, especially in the presence of LLJs (Delgado et al. 2014). The present study confirms previous studies (e.g., Banta et al. 2007) that turbulence in a thick nocturnal boundary layer can be significant in the presence of strong LLJs. As a result, the vertical distribution of meteorological and chemical variables may be significantly modulated. In case of ozone, during quiescent nights, surface ozone normally decreases through the evening due to dry deposition and chemical reactions. In the presence of strong LLJs, however, strong turbulence plays an important role in transporting ozone-richer residual layer air to the surface leading to nocturnal surface ozone peaks (Hu et al. 2013a, Klein et al. 2014). Given the impact of LLJs on vertical redistribution, the traditional understanding of horizontal

transport of atmospheric and chemical scalars in the nocturnal boundary layer and its contribution to the downwind meteorological and chemical processes needs to be improved.

The improved understanding of the NBL also has important implications for future model improvement. Model biases for near-surface wind, temperature, and pollutants (e.g., ozone) during nighttime are often reported. Systematic over-estimations of near-surface winds during stable conditions have been noted in the simulations with several meteorological models (e.g., Zhang and Zheng 2004, Miao et al. 2008, Han et al. 2008, Shimada et al. 2011, Vautard et al. 2012, Garcia-Menendez et al. 2013, Zhang et al. 2013, Wang and Jin 2013). Such model biases are partially due to inaccurate coupling strength in the nocturnal boundary layer simulated by PBL parameterization schemes (Banta et al. 2007, Hu et al. 2013a, Holtslag et al. 2013, Sandu et al. 2013). Some PBL schemes give too strong coupling at night, thus systematically overestimating nighttime near-surface temperature and wind speed (Zhang et al. 2013, Hu et al. 2013a, Ngan et al. 2013). Given the vital importance of PBL schemes for accurate simulations of wind, turbulence, and air quality in the lower atmosphere, evaluation of model simulations with different PBL schemes in terms of their nocturnal coupling strength, along with the collection of more suitable observations (e.g., vertical profiles of meteorological and chemical variables from Doppler, Raman, and differential absorption lidars), is warranted for providing guidance to future model improvement.

Acknowledgements. This work was supported by funding from the Office of the Vice President for Research at the University of Oklahoma. The first author was also supported through the NSF Career award ILREUM (NSF ATM 0547882) and NSF grant AGS-1359698. The fourth author was also supported by NSF grants OCI-0905040, AGS-0802888, AGS-0750790, AGS-0941491, AGS-1046171, and AGS-1046081. WRF simulations were performed at the Texas Advanced Computing Center.

References:

Acevedo OC, Costa FD, Degrazia GA (2012) The Coupling State of an Idealized Stable Boundary Layer. Boundary-Layer Meteorology 145 (1):211-228. doi:10.1007/s10546-011-9676-3

Acevedo OC, Fitzjarrald DR (2001) The early evening surface-layer transition: Temporal and spatial variability. Journal of the Atmospheric Sciences 58 (17):2650-2667. doi:10.1175/1520-0469(2001)0582.0.CO;2

Allwine KJ Overview of Joint Urban 2003-An atmospheric dispersion study in Oklahoma City. In: *Joint session between the 8th Symposium on Integrated Observing and Assimilation Systems in the Atmosphere, Oceans and Land Surface and the Symposium on Planning, Nowcasting, and Forecasting in the Urban Zone*, Seattle, WA, 2004. American Meteorological Society,

Baas P, Bosveld FC, Baltink HK, Holtslag AAM (2009) A Climatology of Nocturnal Low-Level Jets at Cabauw. Journal of Applied Meteorology and Climatology 48 (8):1627-1642. doi:10.1175/2009jamc1965.1

Banta RM (2008) Stable-boundary-layer regimes from the perspective of the low-level jet. Acta Geophysica 56 (1):58-87. doi:10.2478/s11600-007-0049-8

Banta RM, Mahrt L, Vickers D, Sun J, Balsley BB, Pichugina YL, Williams EL (2007) The very stable boundary layer on nights with weak low-level jets. Journal of the Atmospheric Sciences 64:3068-3090. doi:10.1175/jas4002.1

Banta RM, Newsom RK, Lundquist JK, Pichugina YL, Coulter RL, Mahrt L (2002) Nocturnal low-level jet characteristics over Kansas during CASES-99. Boundary-Layer Meteorology 105 (2):221-252. doi:10.1023/a:1019992330866

Banta RM, Pichugina YL, Brewer WA (2006) Turbulent velocity-variance profiles in the stable boundary layer generated by a nocturnal low-level jet. Journal of the Atmospheric Sciences 63 (11):2700-2719. doi:10.1175/jas3776.1

Banta RM, Pichugina YL, Kelley ND, Hardesty RM, Brewer WA (2013) Wind Energy Meteorology: Insight into Wind Properties in the Turbine-Rotor Layer of the Atmosphere from High-Resolution Doppler Lidar. Bulletin of the American Meteorological Society 94 (6):883-902. doi:10.1175/bams-d-11-00057.1

Banta RM, Pichugina YL, Newsom RK (2003) Relationship between low-level jet properties and turbulence kinetic energy in the nocturnal stable boundary layer. Journal of the Atmospheric Sciences 60 (20):2549-2555. doi:10.1175/1520-0469(2003)060<2549:rbljpa>2.0.co;2

Belusic D, Guttler I (2010) Can mesoscale models reproduce meandering motions? Quarterly Journal of the Royal Meteorological Society 136 (648):553-565. doi:10.1002/qj.606

Blackadar AK (1957) Boundary layer wind maxima and their significance for the growth of nocturnal inversions. Bulletin of the American Meteorological Society 38:283-290

Bodine D, Klein PM, Arms SC, Shapiro A (2009) Variability of Surface Air Temperature over Gently Sloped Terrain. Journal of Applied Meteorology and Climatology 48 (6):1117-1141. doi:10.1175/2009jamc1933.1

Bonin TA, Blumberg WG, Klein PM, Chilson PB (2015) Thermodynamic and Kinematic Characteristics of the Southern Great Plains Nocturnal Boundary Layer under Differing Turbulence Regimes. Boundary Layer Meteorology

Bonner W (1968) Climatology of Low Level Jet. Monthly Weather Review 96 (12):833-&. doi:10.1175/1520-0493(1968)096<0833:COTLLJ>2.0.CO;2

Bosveld F, Baas P, Steeneveld G, Holtslag A, Angevine W, Bazile E, de Bruijn E, Deacu D, Edwards J, Ek M, Larson V, Pleim J, Raschendorfer M, Svensson G (2014) The Third GABLS Intercomparison Case for Evaluation Studies of Boundary-Layer Models. Part B: Results and Process Understanding. Boundary-Layer Meteorology 152 (2):157-187. doi:10.1007/s10546-014-9919-1

Chambers S, Williams AG, Zahorowski W, Griffiths A, Crawford J (2011) Separating remote fetch and local mixing influences on vertical radon measurements in the lower atmosphere. Tellus Series B-Chemical and Physical Meteorology 63 (5):843-859. doi:10.1111/j.1600-0889.2011.00565.x

Chen F, Kusaka H, Bornstein R, Ching J, Grimmond C, Grossman-Clarke S, Loridan T, Manning K, Martilli A, Miao S, Sailor D, Salamanca F, Taha H, Tewari M, Wang X, Wyszogrodzki A, Zhang C (2011) The integrated WRF/urban modelling system: development, evaluation, and applications to urban environmental problems. International Journal of Climatology 31 (2):273-288. doi:DOI 10.1002/joc.2158

Chen J, Mao H, Talbot RW, Griffin RJ (2006) Application of the CACM and MPMPO modules using the CMAQ model for the eastern United States. Journal of Geophysical Research-Atmospheres 111 (D23). doi:10.1029/2006jd007603

Chen J, Vaughan J, Avise J, O'Neill S, Lamb B (2008) Enhancement and evaluation of the AIRPACT ozone and PM2.5 forecast system for the Pacific Northwest. Journal of Geophysical Research-Atmospheres 113 (D14). doi:10.1029/2007jd009554

Conangla L, Cuxart J (2006) On the turbulence in the upper part of the low-level jet: An experimental and numerical study. Boundary-Layer Meteorology 118 (2):379-400. doi:10.1007/s10546-005-0608-y

Cuxart J, Jimenez M (2007) Mixing processes in a nocturnal low-level jet: An LES study. Journal of the Atmospheric Sciences 64 (5):1666-1679. doi:10.1175/JAS3903.1

De Wekker SFJ, Berg LK, Allwine J, Doran JC, Shaw WJ (2004) Boundary-layer structure upwind and downwind of Oklahoma City during the Joint Urban 2003 field study. Paper presented at the Fifth Conference on Urban Environment, American Meteorological Society, Vancouver, BC, Canada, ,

Delgado R, Rabenhorst S, Demoz B, Hoff RM (2014) Elastic lidar measurements of summer nocturnal low level jet events over Baltimore, Maryland. Journal of Atmospheric Chemistry:1-23. doi:10.1007/s10874-013-9277-2

Deppe A, Gallus W, Takle E (2013) A WRF Ensemble for Improved Wind Speed Forecasts at Turbine Height. Weather and Forecasting 28 (1):212-228. doi:10.1175/WAF-D-11-00112.1

Draxl C, Hahmann A, Pena A, Giebel G (2014) Evaluating winds and vertical wind shear from Weather Research and Forecasting model forecasts using seven planetary boundary layer schemes. Wind Energy 17 (1):39-55. doi:10.1002/we.1555

Duarte H, Leclerc M, Zhang G (2012) Assessing the shear-sheltering theory applied to low-level jets in the nocturnal stable boundary layer. Theoretical and Applied Climatology 110 (3):359-371. doi:10.1007/s00704-012-0621-2

767 Dudhia J (1989) Numerical Study of Convection Observed During the Winter Monsoon Experiment
768 Using a Mesoscale 2-Dimenional Model. Journal of the Atmospheric Sciences 46 (20):3077-3107.
769 doi:10.1175/1520-0469(1989)046<3077:NSOCOD>2.0.CO;2
770
771 Edwards J, Basu S, Bosveld F, Holtslag A (2014) The Impact of Radiation on the GABLS3 Large-Eddy
772 Simulation through the Night and during the Morning Transition. Boundary-Layer Meteorology
773 152 (2):189-211. doi:10.1007/s10546-013-9895-x
774
775 Engardt M (2008) Modelling of near-surface ozone over South Asia. Journal of Atmospheric
776 Chemistry 59 (1):61-80. doi:10.1007/s10874-008-9096-z
777
778 Fast J, McCorcle M (1990) A 2-Dimensional Numerical Sensitivity Study of the Great-Plains Low-Level
779 Jet. Monthly Weather Review 118 (1):151-163. doi:10.1175/1520-
780 0493(1990)118<0151:ATDNSS>2.0.CO;2
781
782 Fernando HJS, Weil JC (2010) Whither the Stable Boundary Layer? A Shift in the Research Agenda.
783 Bulletin of the American Meteorological Society 91 (11):1475-1484.
784 doi:10.1175/2010bams2770.1
785
786 Fiebrich CA, Crawford KC (2001) The impact of unique meteorological phenomena detected by the
787 Oklahoma Mesonet and ARS Micronet on automated quality control. Bulletin of the American
788 Meteorological Society 82 (10):2173-2187. doi:10.1175/1520-0477(2001)0822.3.CO;2
789
790 Foken T (2006) 50 years of the Monin-Obukhov similarity theory. Boundary-Layer Meteorology 119
791 (3):431-447. doi:10.1007/s10546-006-9048-6
792
793 Garcia-Menendez F, Hu Y, Odman M (2013) Simulating smoke transport from wildland fires with a
794 regional-scale air quality model: Sensitivity to uncertain wind fields. Journal of Geophysical
795 Research-Atmospheres 118 (12):6493-6504. doi:10.1002/jgrd.50524
796
797 Grimmond CSB, Su H-B, Offerle B, Crawford B, Scott S, Zhong S, Clements C (2004) Variability of
798 sensible heat fluxes in a suburban area of Oklahoma City. Paper presented at the Symp. on
799 Planning, Nowcasting, and Forecasting in the Urban Zone/Eighth Symp. on Integrated Observing
800 and Assimilation Systems for Atmosphere, Oceans, and Land Surface, Seattle, WA, USA,
801
802 Ha K, Mahrt L (2001) Simple inclusion of z-less turbulence within and above the modeled nocturnal
803 boundary layer. Monthly Weather Review 129 (8):2136-2143. doi:10.1175/1520-
804 0493(2001)129<2136:SIOZLT>2.0.CO;2
805
806 Han Z, Ueda H, An J (2008) Evaluation and intercomparison of meteorological predictions by five
807 MM5-PBL parameterizations in combination with three land-surface models. Atmospheric
808 Environment 42 (2):233-249. doi:10.1016/j.atmosenv.2007.09.053
809
810 Helmis C, Wang Q, Sgouros G, Wang S, Halios C (2013) Investigating the Summertime Low-Level Jet
811 Over the East Coast of the USA: A Case Study. Boundary-Layer Meteorology 149 (2):259-276.
812 doi:10.1007/s10546-013-9841-y
813
814 Holton JR (1967) Diurnal Boundary Layer Wind Oscillation Above Sloping Terrain. Tellus 19 (2):199-
815 &
816
817 Holtslag AAM, Svensson G, Baas P, Basu S, Beare B, Beljaars ACM, Bosveld FC, Cuxart J, Lindvall J,
818 Steeneveld GJ, Tjernstrom M, Van de Wiel BJH (2013) Stable Atmospheric Boundary Layers And
819 Diurnal Cycles - Challenges for Weather and Climate Models. Bulletin of the American
820 Meteorological Society 94 (11):1691-1706. doi:10.1175/bams-d-11-00187.1
821

822 Hong S-Y (2010) A new stable boundary-layer mixing scheme and its impact on the simulated East
823 Asian summer monsoon. Quarterly Journal of the Royal Meteorological Society 136 (651):1481-
824 1496. doi:10.1002/qj.665
825
826 Hong S-Y, Noh Y, Dudhia J (2006) A new vertical diffusion package with an explicit treatment of
827 entrainment processes. Monthly Weather Review 134 (9):2318-2341. doi:10.1175/mwr3199.1
828
829 Hong SY, Dudhia J, Chen SH (2004) A revised approach to ice microphysical processes for the bulk
830 parameterization of clouds and precipitation. Monthly Weather Review 132 (1):103-120.
831 doi:10.1175/1520-0493(2004)132<0103:aratim>2.0.co;2
832
833 Hu X-M, Doughty DC, Sanchez KJ, Joseph E, Fuentes JD (2012) Ozone variability in the atmospheric
834 boundary layer in Maryland and its implications for vertical transport model. Atmospheric
835 Environment 46:354-364. doi:10.1016/j.atmosenv.2011.09.054
836
837 Hu X-M, Fuentes JD, Zhang F (2010) Downward transport and modification of tropospheric ozone
838 through moist convection. Journal of Atmospheric Chemistry 65 (1):13-35. doi:10.1007/s10874-
839 010-9179-5
840
841 Hu X-M, Klein PM, Xue M (2013a) Evaluation of the updated YSU planetary boundary layer scheme
842 within WRF for wind resource and air quality assessments. Journal of Geophysical Research-
843 Atmospheres 118 (18):10,490- 410,505. doi:doi:10.1002/jgrd.50823, 2013
844
845 Hu X-M, Klein PM, Xue M, Lundquist JK, Zhang F, Qi Y (2013b) Impact of Low-Level Jets on the
846 Nocturnal Urban Heat Island Intensity in Oklahoma City. Journal of Applied Meteorology and
847 Climatology 52 (8):1779-1802. doi:10.1175/jamc-d-12-0256.1
848
849 Hu X-M, Klein PM, Xue M, Shapiro A, Nallapareddy A (2013c) Enhanced vertical mixing associated
850 with a nocturnal cold front passage and its impact on near-surface temperature and ozone
851 concentration. Journal of Geophysical Research-Atmospheres 118 (7):2714-2728.
852 doi:10.1002/jgrd.50309
853
854 Hu X-M, Klein PM, Xue M, Zhang F, Doughty DC, Forkel R, Joseph E, Fuentes JD (2013d) Impact of the
855 vertical mixing induced by low-level jets on boundary layer ozone concentration. Atmospheric
856 Environment 70:123-130. doi:10.1016/j.atmosenv.2012.12.046
857
858 Jiang X, Lau N-C, Held IM, Ploshay JJ (2007) Mechanisms of the great plains low-level jet as simulated
859 in an AGCM. Journal of the Atmospheric Sciences 64 (2):532-547. doi:10.1175/jas3847.1
860
861 Kallistratova M, Kouznetsov R, Kuznetsov D, Kuznetsova I, Nakhaev M, Chirokova G (2009)
862 Summertime low-level jet characteristics measured by sodars over rural and urban areas.
863 Meteorologische Zeitschrift 18 (3):289-295. doi:10.1127/0941-2948/2009/0380
864
865 Karipot A, Leclerc MY, Zhang G, Lewin KF, Nagy J, Hendrey GR, Starr G (2008) Influence of nocturnal
866 low-level jet on turbulence structure and CO2 flux measurements over a forest canopy. Journal of
867 Geophysical Research-Atmospheres 113 (D10). doi:10.1029/2007jd009149
868
869 Klein P, Bonin TA, Newman JF, Turner DD, Chilson PB, Wainwright CE, Blumberg WG, Mishra S,
870 Carney M, Jacobsen EP, Wharton S, Newsom RK (2015) LABLE: A multi-institutional, student-led,
871 atmospheric boundary-layer experiment. Bulletin of the American Meteorological Society e-View.
872 doi:10.1175/BAMS-D-13-00267.1
873
874 Klein PM, Hu X-M, Xue M (2014) Impacts of Mixing Processes in Nocturnal Atmospheric Boundary
875 Layer on Urban Ozone Concentrations. Boundary-Layer Meteorology 150 (1):107-130. doi:DOI
876 10.1007/s10546-013-9864-4

Kutsher J, Haikin N, Sharon A, Heifetz E (2012) On the Formation of an Elevated Nocturnal Inversion Layer in the Presence of a Low-Level Jet: A Case Study. Boundary-Layer Meteorology 144 (3):441-449. doi:10.1007/s10546-012-9720-y

Lareau N, Crosman E, Whiteman C, Horel J, Hoch S, Brown W, Horst T (2013) The Persistent Cold-Air Pool study. Bulletin of the American Meteorological Society 94 (1):51-63. doi:10.1175/BAMS-D-11-00255.1

Lemonsu A, Belair S, Mailhot J (2009) The New Canadian Urban Modelling System: Evaluation for Two Cases from the Joint Urban 2003 Oklahoma City Experiment. Boundary-Layer Meteorology 133 (1):47-70. doi:DOI 10.1007/s10546-009-9414-2

Lin J, McElroy M (2010) Impacts of boundary layer mixing on pollutant vertical profiles in the lower troposphere: Implications to satellite remote sensing. Atmospheric Environment 44 (14):1726-1739. doi:10.1016/j.atmosenv.2010.02.009

Liu Y, Chen F, Warner T, Basara J (2006) Verification of a mesoscale data-assimilation and forecasting system for the Oklahoma City area during the Joint Urban 2003 field project. Journal of Applied Meteorology and Climatology 45 (7):912-929. doi:10.1175/JAM2383.1

Lundquist J (2003) Intermittent and elliptical inertial oscillations in the atmospheric boundary layer. Journal of the Atmospheric Sciences 60 (21):2661-2673. doi:10.1175/1520-0469(2003)060<2661:IAEIOI>2.0.CO;2

Lundquist J, Mirocha J (2008) Interaction of nocturnal low-level jets with urban geometries as seen in joint urban 2003 data. Journal of Applied Meteorology and Climatology 47 (1):44-58. doi:10.1175/2007JAMC1581.1

Mahrt L (1999) Stratified atmospheric boundary layers. Boundary-Layer Meteorology 90 (3):375-396. doi:10.1023/a:1001765727956

Mahrt L (2007) Weak-wind mesoscale meandering in the nocturnal boundary layer. Environmental Fluid Mechanics 7 (4):331-347. doi:10.1007/s10652-007-9024-9

Mahrt L (2009) Characteristics of Submeso Winds in the Stable Boundary Layer. Boundary-Layer Meteorology 130 (1):1-14. doi:10.1007/s10546-008-9336-4

Mahrt L (2010) Variability and Maintenance of Turbulence in the Very Stable Boundary Layer. Boundary-Layer Meteorology 135 (1):1-18. doi:10.1007/s10546-009-9463-6

Mahrt L (2011) Surface Wind Direction Variability. Journal of Applied Meteorology and Climatology 50 (1):144-152. doi:10.1175/2010jamc2560.1

Mahrt L (2014) Stably Stratified Atmospheric Boundary Layers. Annual Review of Fluid Mechanics, Vol 46 46:23-45. doi:10.1146/annurev-fluid-010313-141354

Mahrt L, Vickers D (2002) Contrasting vertical structures of nocturnal boundary layers. Boundary-Layer Meteorology 105 (2):351-363. doi:10.1023/a:1019964720989

Mahrt L, Vickers D, Andreas EL (2014) Low-Level Wind Maxima and Structure of the Stably Stratified Boundary Layer in the Coastal Zone. Journal of Applied Meteorology and Climatology 53 (2):363-376. doi:10.1175/jamc-d-13-0170.1

931 Mao Q, Gautney LL, Cook TM, Jacobs ME, Smith SN, Kelsoe JJ (2006) Numerical experiments on MM5-
932 CMAQ sensitivity to various PBL schemes. Atmospheric Environment 40 (17):3092-3110.
933 doi:10.1016/j.atmosenv.2005.12.055
934
935 McPherson RA, Fiebrich CA, Crawford KC, Elliott RL, Kilby JR, Grimsley DL, Martinez JE, Basara JB,
936 Illston BG, Morris DA, Kloesel KA, Stadler SJ, Melvin AD, Sutherland AJ, Shrivastava H, Carlson JD,
937 Wolfinbarger JM, Bostic JP, Demko DB (2007) Statewide monitoring of the mesoscale
938 environment: A technical update on the Oklahoma Mesonet. Journal of Atmospheric and Oceanic
939 Technology 24 (3):301-321. doi:10.1175/jtech1976.1
940
941 Miao JF, Chen D, Wyser K, Borne K, Lindgren J, Strandevall MKS, Thorsson S, Achberger C, Almkvist E
942 (2008) Evaluation of MM5 mesoscale model at local scale for air quality applications over the
943 Swedish west coast: Influence of PBL and LSM parameterizations. Meteorology and Atmospheric
944 Physics 99 (1-2):77-103. doi:10.1007/s00703-007-0267-2
945
946 Mitchell MJ, Arritt RW, Labas K (1995) A Climatology of the Warm-Season Great-Plains Low-Level Jet
947 Using Wind Profiler Observations. Weather and Forecasting 10 (3):576-591. doi:10.1175/1520-
948 0434(1995)010<0576:acotws>2.0.co;2
949
950 Mlawer EJ, Taubman SJ, Brown PD, Iacono MJ, Clough SA (1997) Radiative transfer for
951 inhomogeneous atmospheres: RRTM, a validated correlated-k model for the longwave. Journal of
952 Geophysical Research-Atmospheres 102 (D14):16663-16682. doi:10.1029/97jd00237
953
954 Newman J, Klein P (2014) The Impacts of Atmospheric Stability on the Accuracy of Wind Speed
955 Extrapolation Methods. Resources 3 (1):81-105
956
957 Ngan F, Kim H, Lee P, Al-Wali K, Dornblaser B (2013) A Study of Nocturnal Surface Wind Speed
958 Overprediction by the WRF-ARW Model in Southeastern Texas. Journal of Applied Meteorology
959 and Climatology 52 (12):2638-2653. doi:10.1175/JAMC-D-13-060.1
960
961 Nielsen-Gammon J, Hu X, Zhang F, Pleim J (2010) Evaluation of Planetary Boundary Layer Scheme
962 Sensitivities for the Purpose of Parameter Estimation. Monthly Weather Review 138 (9):3400-
963 3417. doi:10.1175/2010MWR3292.1
964
965 Nunalee C, Basu S (2014) Mesoscale modeling of coastal low-level jets: implications for offshore wind
966 resource estimation. Wind Energy 17 (8):1199-1216. doi:10.1002/we.1628
967
968 Ohya Y, Nakamura R, Uchida T (2008) Intermittent bursting of turbulence in a stable boundary layer
969 with low-level jet. Boundary-Layer Meteorology 126 (3):349-363. doi:10.1007/s10546-007-
970 9245-y
971
972 Pan Z, Segal M, Arritt R (2004) Role of topography in forcing low-level jets in the Central United
973 States during the 1993 flood-altered terrain simulations. Monthly Weather Review 132 (1):396-
974 403. doi:10.1175/1520-0493(2004)132<0396:ROTIFL>2.0.CO;2
975
976 Parish T, Oolman L (2010) On the Role of Sloping Terrain in the Forcing of the Great Plains Low-Level
977 Jet. Journal of the Atmospheric Sciences 67 (8):2690-2699. doi:10.1175/2010JAS3368.1
978
979 Pichugina Y, Banta R (2010) Stable Boundary Layer Depth from High-Resolution Measurements of
980 the Mean Wind Profile. Journal of Applied Meteorology and Climatology 49 (1):20-35.
981 doi:10.1175/2009JAMC2168.1
982
983 Pu B, Dickinson R (2014) Diurnal Spatial Variability of Great Plains Summer Precipitation Related to
984 the Dynamics of the Low-Level Jet. Journal of the Atmospheric Sciences 71 (5):1807-1817.
985 doi:10.1175/JAS-D-13-0243.1

Sandu I, Beljaars A, Bechtold P, Mauritsen T, Balsamo G (2013) Why is it so difficult to represent stably stratified conditions in numerical weather prediction (NWP) models? Journal of Advances in Modeling Earth Systems 5 (2):117-133. doi:10.1002/jame.20013

Schroter J, Moene A, Holtslag A (2013) Convective boundary layer wind dynamics and inertial oscillations: the influence of surface stress. Quarterly Journal of the Royal Meteorological Society 139 (676):1694-1711. doi:10.1002/qj.2069

Shapiro A, Fedorovich E (2009) Nocturnal low-level jet over a shallow slope. Acta Geophysica 57 (4). doi:10.2478/s11600-009-0026-5

Shapiro A, Fedorovich E (2010) Analytical description of a nocturnal low-level jet. Quarterly Journal of the Royal Meteorological Society 136 (650). doi:10.1002/qj.628

Shibuya R, Sato K, Nakanishi M (2014) Diurnal Wind Cycles Forcing Inertial Oscillations: A Latitude-Dependent Resonance Phenomenon. Journal of the Atmospheric Sciences 71 (2):767-781. doi:10.1175/jas-d-13-0124.1

Shimada S, Ohsawa T (2011) Accuracy and Characteristics of Offshore Wind Speeds Simulated by WRF. Sola 7. doi:10.2151/sola.2011-006

Shin H, Hong S (2011) Intercomparison of Planetary Boundary-Layer Parametrizations in the WRF Model for a Single Day from CASES-99. Boundary-Layer Meteorology 139 (2):261-281. doi:10.1007/s10546-010-9583-z

Skamarock WC, Klemp JB, Dudhia J, Gill DO, Barker DM, Duda MG, Huang XY, Wang W, Powers JG (2008) A Description of the Advanced Research WRF Version 3. NCAR TECHNICAL NOTE. National Center for Atmospheric Research Boulder, CO, USA

Smedman A, Bergstrom H, Grisogono B (1997) Evolution of stable internal boundary layers over a cold sea. Journal of Geophysical Research-Oceans 102 (C1):1091-1099. doi:10.1029/96JC02782

Smedman A, Bergstrom H, Hogstrom U (1995) Spectra, variances and length scales in a marine stable boundary layer dominated by a low level jet. Boundary-Layer Meteorology 76 (3):211-232. doi:10.1007/BF00709352

Song J, Liao K, Coulter R, Lesht B (2005) Climatology of the low-level jet at the southern Great Plains atmospheric Boundary Layer Experiments site. Journal of Applied Meteorology 44 (10):1593-1606. doi:10.1175/JAM2294.1

Stensrud D (1996) Importance of low-level jets to climate: A review. Journal of Climate 9 (8):1698-1711. doi:10.1175/1520-0442(1996)009<1698:IOLLJT>2.0.CO;2

Storm B, Dudhia J, Basu S, Swift A, Giammanco I (2009) Evaluation of the Weather Research and Forecasting Model on Forecasting Low-level Jets: Implications for Wind Energy. Wind Energy 12 (1):81-90. doi:10.1002/we.288

Sun J, Mahrt L, Banta R, Pichugina Y (2012) Turbulence Regimes and Turbulence Intermittency in the Stable Boundary Layer during CASES-99. Journal of the Atmospheric Sciences 69 (1):338-351. doi:10.1175/JAS-D-11-082.1

Van de Wiel B, Moene A, Jonker H (2012a) The Cessation of Continuous Turbulence as Precursor of the Very Stable Nocturnal Boundary Layer. Journal of the Atmospheric Sciences 69 (11):3097-3115. doi:10.1175/JAS-D-12-064.1

Van de Wiel B, Moene A, Jonker H, Baas P, Basu S, Donda J, Sun J, Holtslag A (2012b) The Minimum Wind Speed for Sustainable Turbulence in the Nocturnal Boundary Layer. Journal of the Atmospheric Sciences 69 (11):3116-3127. doi:10.1175/JAS-D-12-0107.1

Van de Wiel B, Moene A, Steeneveld G, Baas P, Bosveld F, Holtslag A (2010) A Conceptual View on Inertial Oscillations and Nocturnal Low-Level Jets. Journal of the Atmospheric Sciences 67 (8):2679-2689. doi:10.1175/2010JAS3289.1

Vautard R, Moran M, Solazzo E, Gilliam R, Matthias V, Bianconi R, Chemel C, Ferreira J, Geyer B, Hansen A, Jericevic A, Prank M, Segers A, Silver J, Werhahn J, Wolke R, Rao S, Galmarini S (2012) Evaluation of the meteorological forcing used for the Air Quality Model Evaluation International Initiative (AQMEII) air quality simulations. Atmospheric Environment 53:15-37. doi:10.1016/j.atmosenv.2011.10.065

Wang C, Jin S (2014) Error features and their possible causes in simulated low-level winds by WRF at a wind farm. Wind Energy 17 (9):1315-1325. doi:10.1002/we.1635

Wang Y, Klipp CL, Garvey DM, Ligon DA, Williamson CC, Chang SS, Newsom RK, Calhoun R (2007) Nocturnal low-level-jet-dominated atmospheric boundary layer observed by a Doppler lidar over Oklahoma City during JU2003. Journal of Applied Meteorology and Climatology 46 (12):2098-2109. doi:10.1175/2006jamc1283.1

Wei W, Wu B, Ye X, Wang H, Zhang H (2013) Characteristics and Mechanisms of Low-Level Jets in the Yangtze River Delta of China. Boundary-Layer Meteorology 149 (3):403-424. doi:10.1007/s10546-013-9852-8

Wei W, Zhang H, Ye X (2014) Comparison of low-level jets along the north coast of China in summer. Journal of Geophysical Research-Atmospheres 119 (16):9692-9706. doi:10.1002/2014JD021476

Werth D, Kurzeja R, Dias N, Zhang G, Duarte H, Fischer M, Parker M, Leclerc M (2011) The Simulation of the Southern Great Plains Nocturnal Boundary Layer and the Low-Level Jet with a High-Resolution Mesoscale Atmospheric Model. Journal of Applied Meteorology and Climatology 50 (7):1497-1513. doi:10.1175/2011JAMC2272.1

Wexler H (1961) A Boundary Layer Interpretation of the Low-Level Jet. Tellus 13 (3):368-378

Williams A, Chambers S, Griffiths A (2013) Bulk Mixing and Decoupling of the Nocturnal Stable Boundary Layer Characterized Using a Ubiquitous Natural Tracer. Boundary-Layer Meteorology 149 (3):381-402. doi:10.1007/s10546-013-9849-3

Yu X, Yuan Z, Fung J, Xue J, Li Y, Zheng J, Lau A (2014) Ozone changes in response to the heavy-duty diesel truck control in the Pearl River Delta. Atmospheric Environment 88:269-274. doi:10.1016/j.atmosenv.2013.11.022

Zhang D, Zhang S, Weaver S (2006) Low-level jets over the Mid-Atlantic states: Warm-season climatology and a case study. Journal of Applied Meteorology and Climatology 45 (1):194-209. doi:10.1175/JAM2313.1

Zhang D, Zheng W (2004) Diurnal cycles of surface winds and temperatures as simulated by five boundary layer parameterizations. Journal of Applied Meteorology 43 (1):157-169. doi:10.1175/1520-0450(2004)043<0157:DCOSWA>2.0.CO;2

1094 Zhang H, Pu Z, Zhang X (2013) Examination of Errors in Near-Surface Temperature and Wind from
1095 WRF Numerical Simulations in Regions of Complex Terrain. Weather and Forecasting 28
1096 (3):893-914. doi:10.1175/WAF-D-12-00109.1
1097
1098 Zhang Y, Dubey M, Olsen S, Zheng J, Zhang R (2009) Comparisons of WRF/Chem simulations in
1099 Mexico City with ground-based RAMA measurements during the 2006-MILAGRO. Atmospheric
1100 Chemistry and Physics 9 (11):3777-3798
1101
1102 Zhong S, Fast J, Bian X (1996) A case study of the great plains low-level jet using wind profiler
1103 network data and a high-resolution mesoscale model. Monthly Weather Review 124 (5):785-806.
1104 doi:10.1175/1520-0493(1996)124<0785:ACSOTG>2.0.CO;2
1105

Table 1. Sigma levels and mid-layer heights (m a.g.l.) of the lowest 20 model layers. The sigma levels are defined as $\frac{p-p_{top}}{p_{surf}-p_{top}}$, where p is the dry hydrostatic pressure at each corresponding level, p_{surf} is dry hydrostatic surface pressure, and p_{top} is a constant dry hydrostatic pressure at model top.

sigma levels	1.0	0.997	0.994	0.991	0.988	0.985	0.975	0.97	0.96	0.95
mid-layer heights	12	37	61	86	111	144	186	227	290	374
sigma levels	0.94	0.93	0.92	0.91	0.895	0.88	0.865	0.85	0.825	0.8
mid-layer heights	459	545	631	717	826	958	1092	1226	1409	1640

Table 2: Summary of LLJ and near surface stability and turbulence parameters observed during the study period. See text for details about the definitions of the parameters. The numbers in the first column refer to the day in July 2003.

Day	$(U_{LLJ})_{max}$ [ms^{-1}]	U_s [ms^{-1}]	$(U_{LLJ}/U_s)_{max}$	$(U_{LLJ}/U_{37})_{max}$	$(U_{80}/U_{37})_{max}$	Ri_{night}	Ri_{day}	$U_{t,night}$ [ms^{-1}]	$U_{t,day}$ [ms^{-1}]	$(U_t/U_{37})_{night}$	$(U_t/U_{37})_{day}$
2	17.2	7.6	2.3	N/A	N/A	0.12	-0.22	N/A	N/A	N/A	N/A
3	14.4	7.8	1.8	N/A	N/A	0.21	-0.17	N/A	N/A	N/A	N/A
5	19.4	8.0	2.4	3.6	1.3	0.08	-0.18	1.0	N/A	0.20	N/A
6	21.7	9.8	2.2	3.9	1.3	0.06	-0.07	1.0	1.7	0.18	0.23
7	21.1	9.9	2.1	3.4	1.4	0.04	-0.12	1.0	1.5	0.19	0.21
8	20.5	9.8	2.1	3.5	1.3	0.07	-0.08	1.1	1.5	0.19	0.21
11	21.0	10.8	2.0	3.5	1.4	0.09	-0.09	1.0	1.6	0.16	0.23
12	19.5	9.8	2.0	3.6	1.4	0.24	-0.26	0.9	1.5	0.17	0.28
13	20.8	10.9	1.9	3.5	1.4	0.07	-0.14	1.1	1.4	0.18	0.22
14	22.5	10.9	2.1	3.2	1.3	0.04	-0.10	1.4	1.6	0.18	0.23
15	17.6	6.8	2.6	3.0	1.4	0.15	-0.21	1.0	1.4	0.18	0.21
16	17.6	8.4	2.1	4.1	1.6	0.18	-0.24	0.7	1.3	0.16	0.25
17	15.1	6.9	2.2	3.6	1.7	0.25	-0.27	0.5	1.3	0.13	0.25
18	16.2	6.6	2.5	4.4	1.7	0.19	-0.37	0.4	1.2	0.12	0.36
24	18.7	7.7	2.4	3.1	1.4	0.04	-0.25	1.0	1.5	0.18	0.24
25	19.0	8.7	2.2	3.2	1.4	0.03	-0.20	1.2	1.5	0.18	0.21
26	18.4	6.9	2.7	3.2	1.3	0.10	-0.37	1.0	1.5	0.18	0.30
27	17.8	6.5	2.7	3.6	1.5	0.11	-0.38	0.8	1.4	0.16	0.30
Max	**22.5**	**10.9**	**2.7**	**4.4**	**1.7**	**0.25**	**-0.07**	**1.4**	**1.7**	**0.20**	**0.36**
Min	**14.4**	**6.5**	**1.8**	**3.0**	**1.3**	**0.03**	**-0.38**	**0.4**	**1.2**	**0.12**	**0.21**

Petra Klein, Xiao-Ming Hu, Alan Shapiro, Ming Xue.
School of Meteorology and Center for Analysis and Prediction of Storms, University of Oklahoma,
120 David L. Boren Blvd., Norman, Oklahoma, 73072, USA, email: pkklein@ou.edu and xhu@ou.edu

Figures

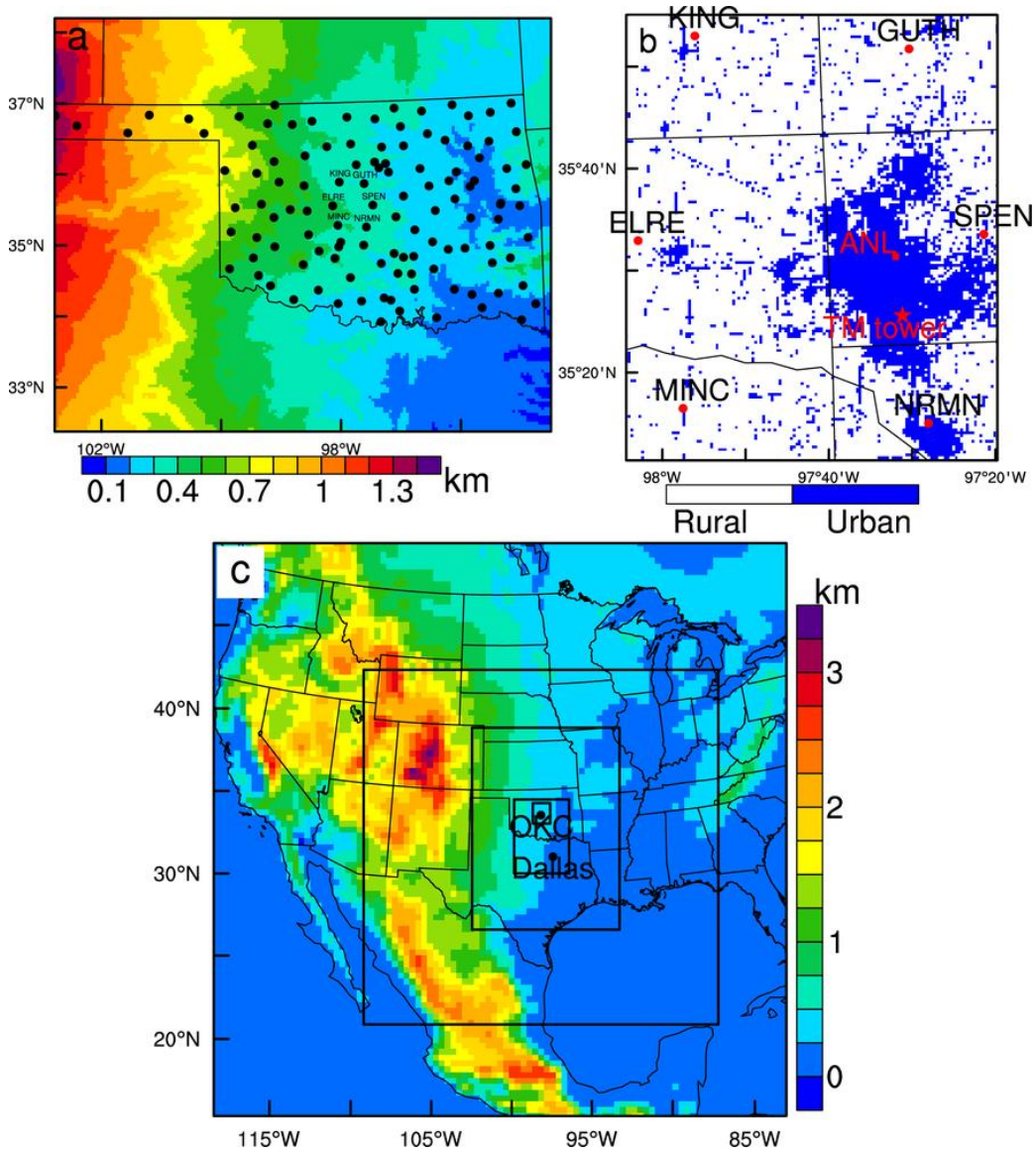

Figure 1. (a) Map of Oklahoma with the locations of all Oklahoma Mesonet sites and (b) land use categories (i.e., rural and urban) over the study area around Oklahoma City retrieved from the 2006 National Land Cover Data. The locations of six rural Mesonet sites around Oklahoma City (i.e., ELRE, GUTH, KING, MINC, NRMN, and SPEN) are marked by dots, the Argonne National Lab (ANL) site is marked by a square, and the Tyler Media (TM) tower is marked by a star on panel (b). The background colour in (a) shows the terrain height in km. (c) Map of model domains and terrain heights (in km) used for the WRF simulations.

Petra Klein, Xiao-Ming Hu, Alan Shapiro, Ming Xue.
School of Meteorology and Center for Analysis and Prediction of Storms, University of Oklahoma,
120 David L. Boren Blvd., Norman, Oklahoma, 73072, USA, email: pkklein@ou.edu and xhu@ou.edu

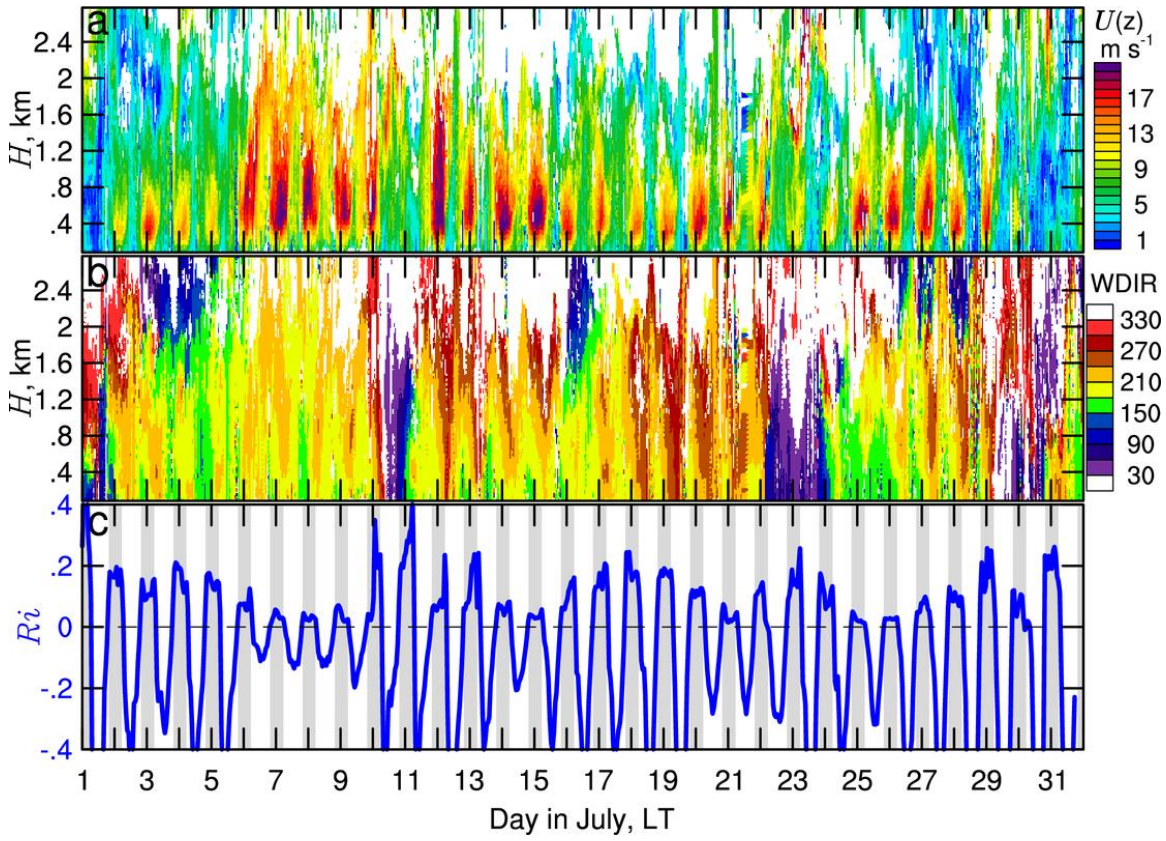

Figure 2. Time-height diagram of (a) wind speed and (b) wind direction in July 2003 at the ANL site observed with a boundary-layer radar wind profiler, and (c) time series of Richardson number (Ri) averaged over six Oklahoma Mesonet sites. Periods of sunset to sunrise (i.e., 1942-0527 CST) are shaded in the middle panel. Note the heights in panels (a) and (c) are above ground level and the daytime values of *Ri* on some days are lower than -0.4, but this lower limit was chosen to better document the *Ri* values during the early-evening transition and at night..

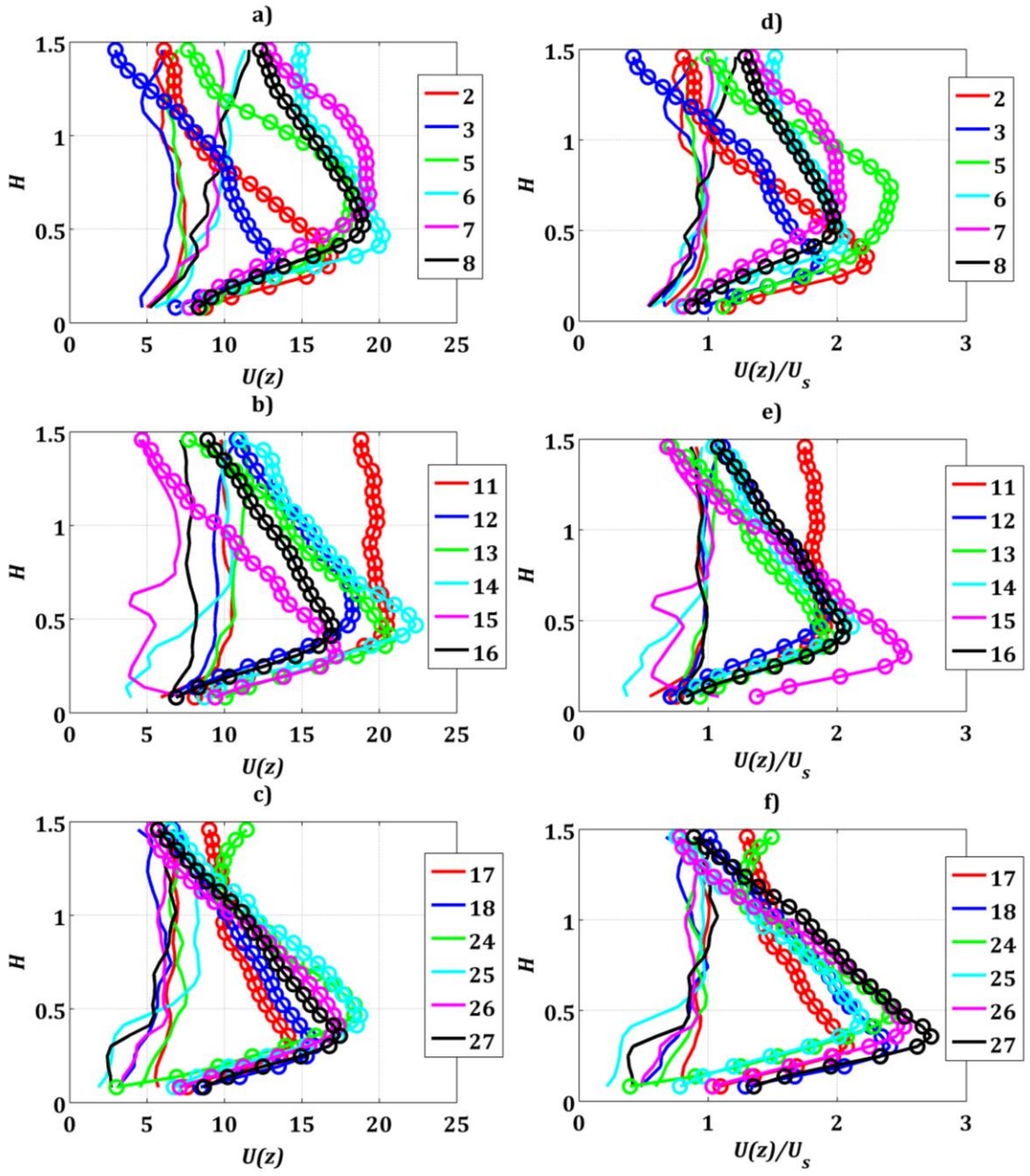

Figure 3. (a-c) Observed averaged daytime and nighttime wind profiles for the 18 days included in the analysis and (d-f) corresponding normalized profiles whereby the wind speed at 800 m above ground from the daytime profile is used as scaling velocity U_s for both daytime (solid lines) and nighttime (solid lines and circles) profiles. The vertical axis refers to the height a.g.l in km. See text for more details.

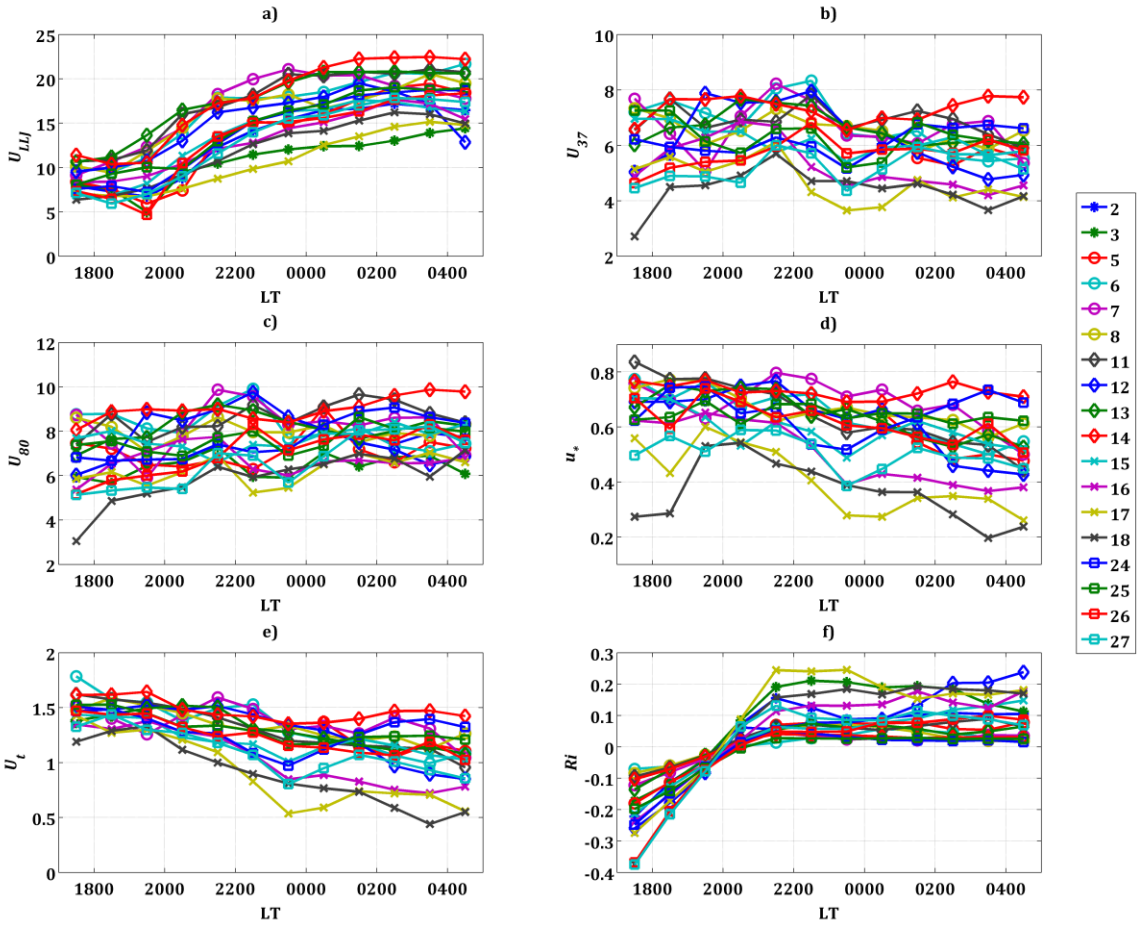

Figure 4. Temporal evolution of (a) LLJ strength U_{LLJ}, (b-c) wind speeds measured with sonic anemometers at the TM tower at 37-m (U_{37}) and 80-m (U_{80}) above ground, (d-e) friction velocity u_* and turbulent velocity scale U_t, both also measured with the 37-m sonic anemometer, and (f) stability parameter *Ri* computed from wind and temperature data at six rural Mesonet sites using Eq. (3). All wind speeds are plotted in m s^{-1} and the legend refers to the day in July 2003.

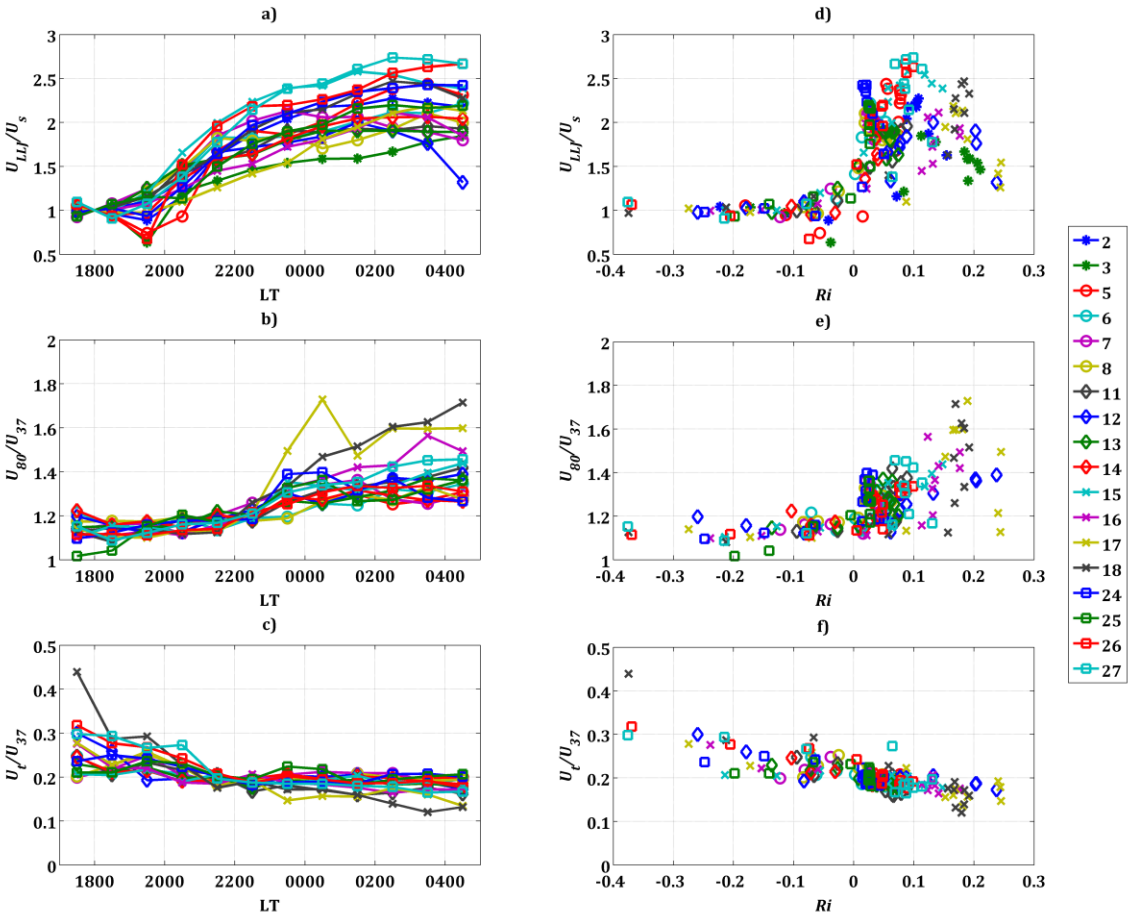

Figure 5. Temporal evolution of (a) relative LLJ strength U_{LLJ}/U_s, (b) wind speed ratio U_{37}/U_{80} which serves as shear parameter, and (c) turbulence intensity U_t/U_{37}. Panels (d-f) show the same three parameters but plotted as a function of the stability parameter Ri instead of as a function of time. The legend refers to the day in July 2003.

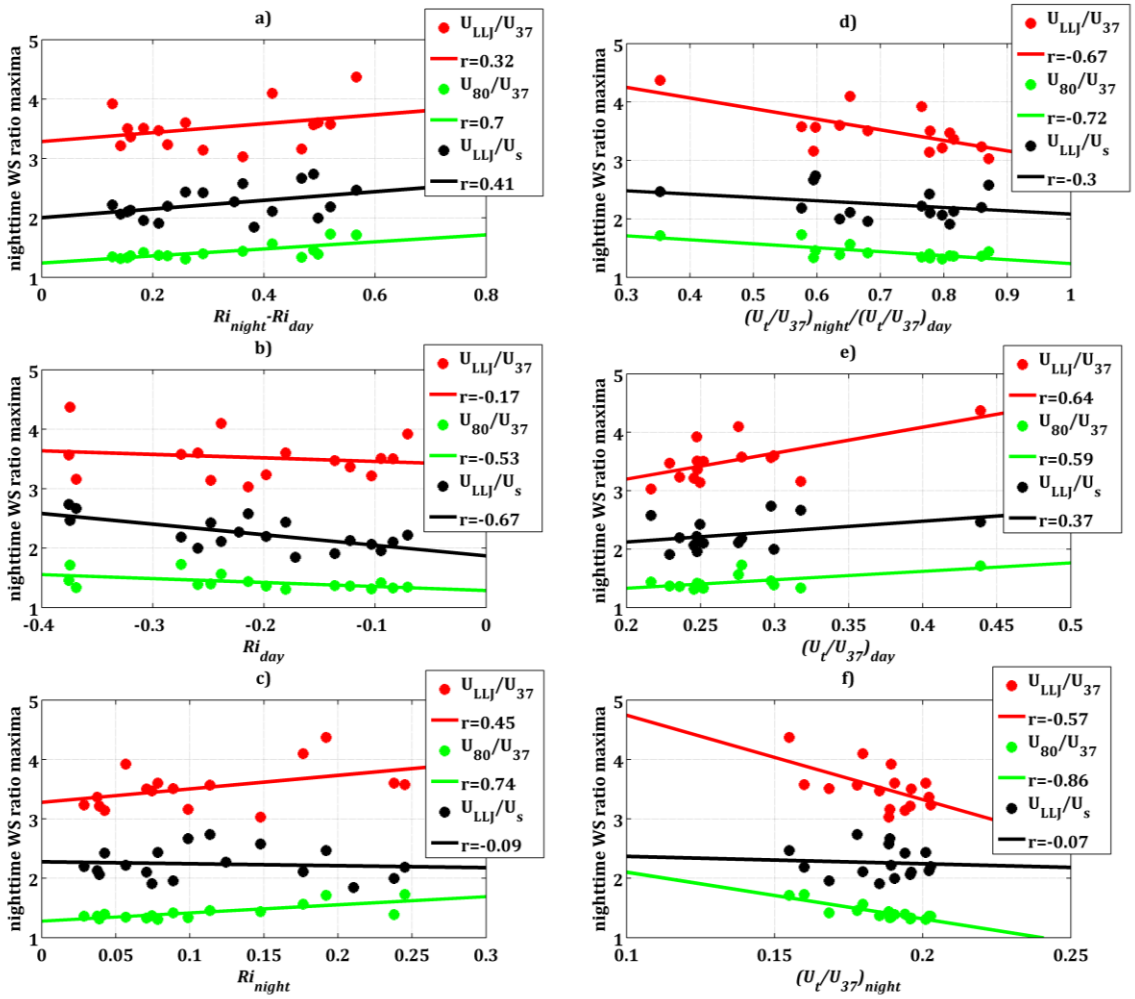

Figure 6. Plots of relative LLJ strength U_{LLJ}/U_s and shear parameters U_{37}/U_{80} and U_{LLJ}/U_{80} versus (a) night-to-day change in stability Ri_{night}- Ri_{day} (b) daytime stability Ri_{day}, (c) nighttime stability Ri_{night}, (d) night-to-day change in turbulence intensity $(U_t/U_{37})_{night}/(U_t/U_{37})_{day}$ (e) daytime turbulence intensity $(U_t/U_{37})_{day}$, and (e) nighttime turbulence intensity $(U_t/U_{37})_{night}$. See text for more details.

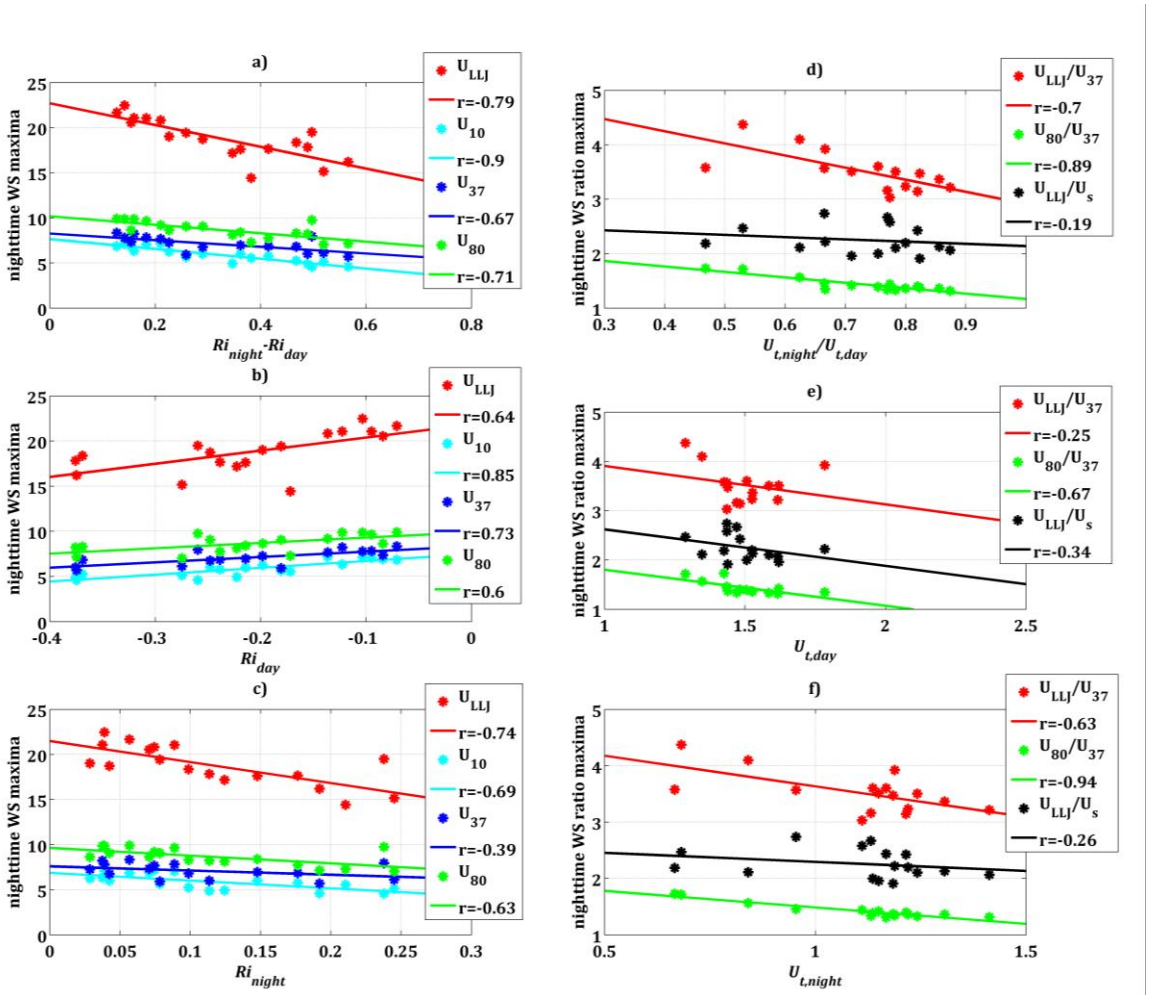

Figure 7. Similar to Fig. 6, but instead of normalized velocities absolute velocities are plotted against (a) night-to-day change in stability Ri_{night}- Ri_{day} (b) daytime stability Ri_{day}, (c) nighttime stability Ri_{night}. In panels (d-f), the normalized velocities are plotted against turbulent velocity scales instead of turbulence intensities. See text for more details.

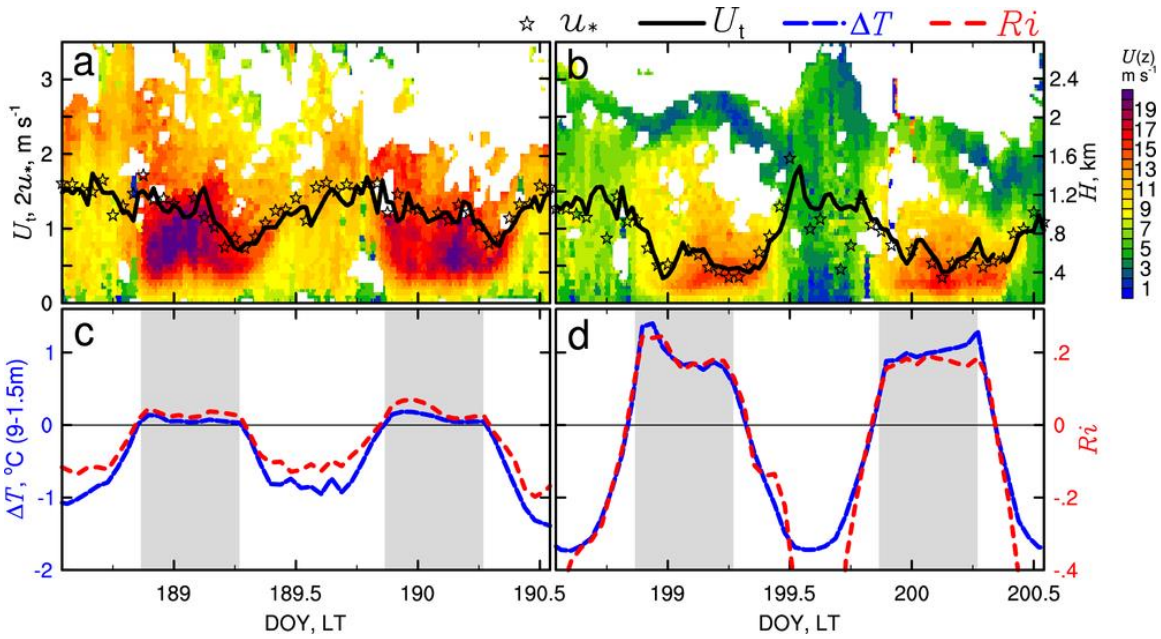

Figure 8. (a,b) Time–height diagram of horizontal wind speed observed by the boundary layer wind profiler overlaid with the time series of turbulent velocity scale U_t and frictional velocity u_* and (c,d) time series of mean inversion strength (ΔT between 1.5 and 9 m) and Ri at the six mesonet sites during the periods of (left) July 7-9 (DOY 188-190) and (right) July 17-19, 2003 (DOY 198-200). Periods of sunset to sunrise are shaded in the bottom panel.

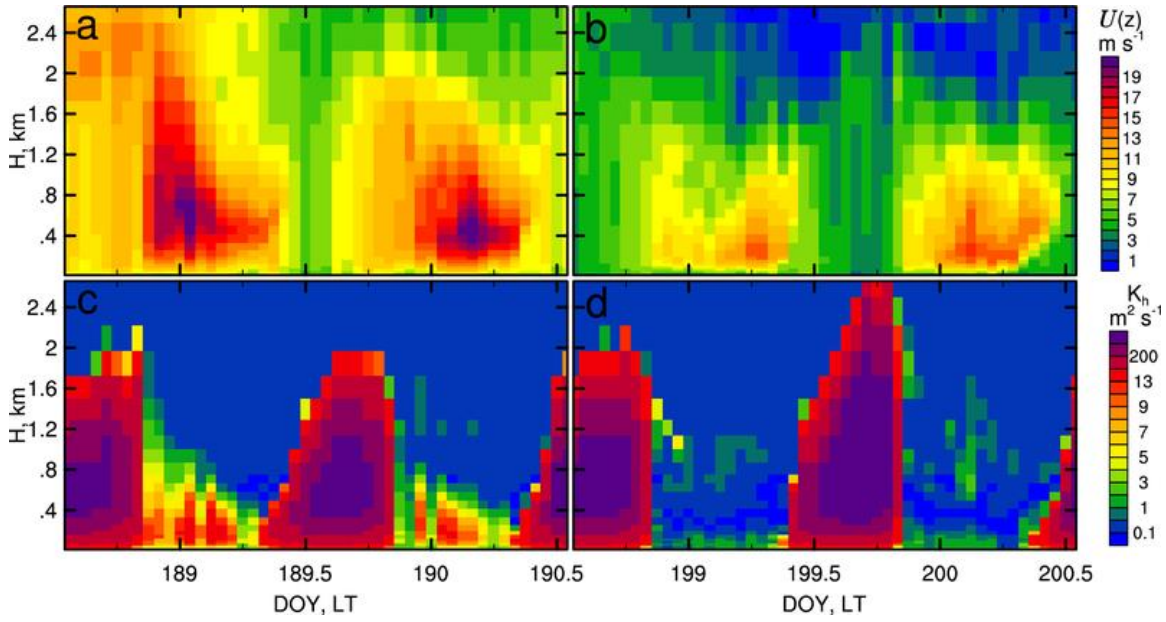

Figure 9. Time-height diagram of (a,b) horizontal wind speed U(z) and (c,d) eddy diffusivity for heat K_h during the periods of (left) July 7-9 (DOY 188-190) and (right) July 17-19, 2003 (DOY 198-200) simulated by WRF with the default YSU PBL scheme (i.e., $a = 5$).

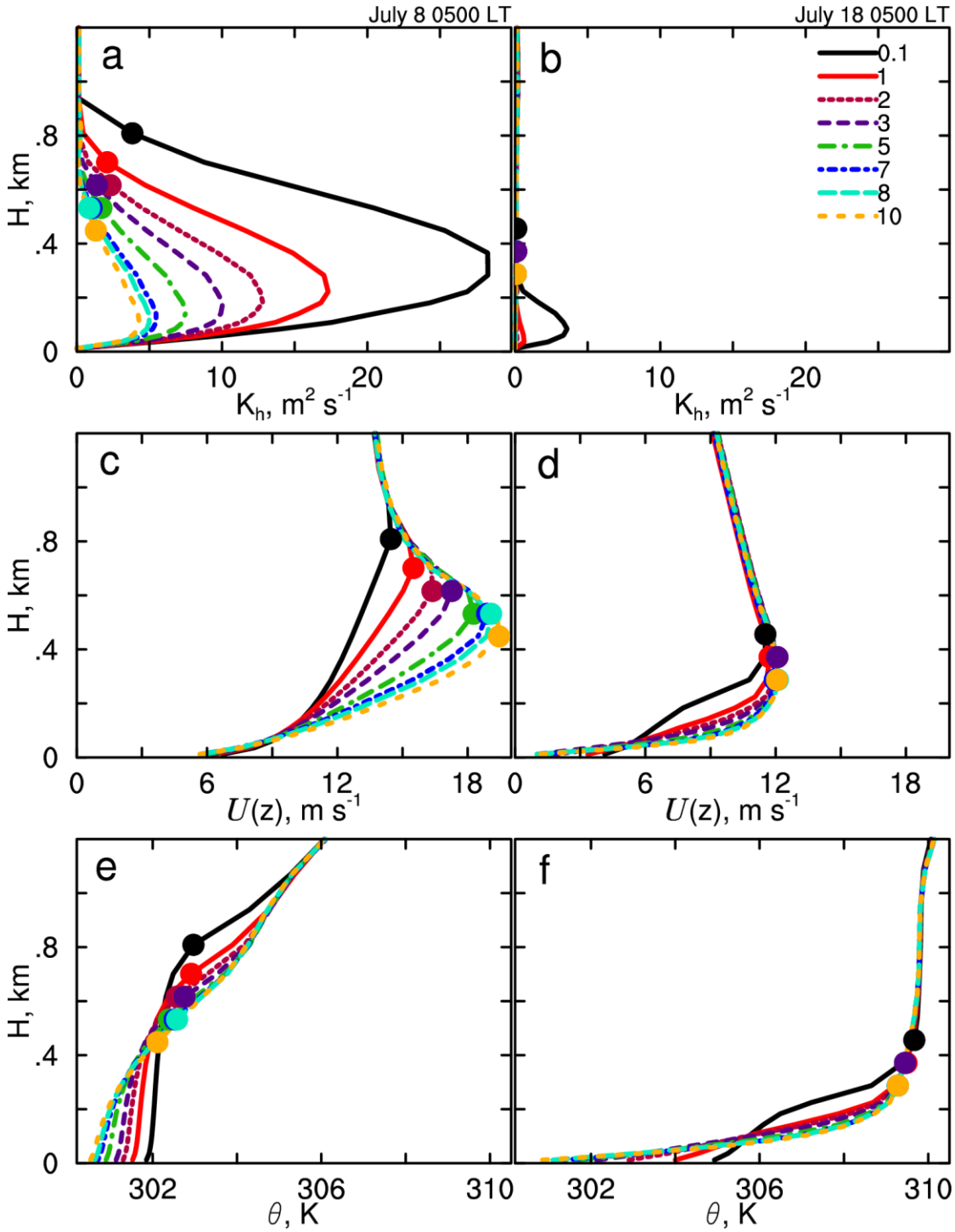

Figure 10. Vertical profiles of (a,b) eddy diffusivity K_h, (c,d) wind speed $U(z)$, and (e,f) potential temperature θ over Oklahoma City at 05 LT on (left) July 8 and (right) July 18, 2003 simulated by WRF with the YSU PBL scheme with the coefficient a of Eq. (5) varying from 0.1 to 10. The locations of the jet noses are marked with dots.

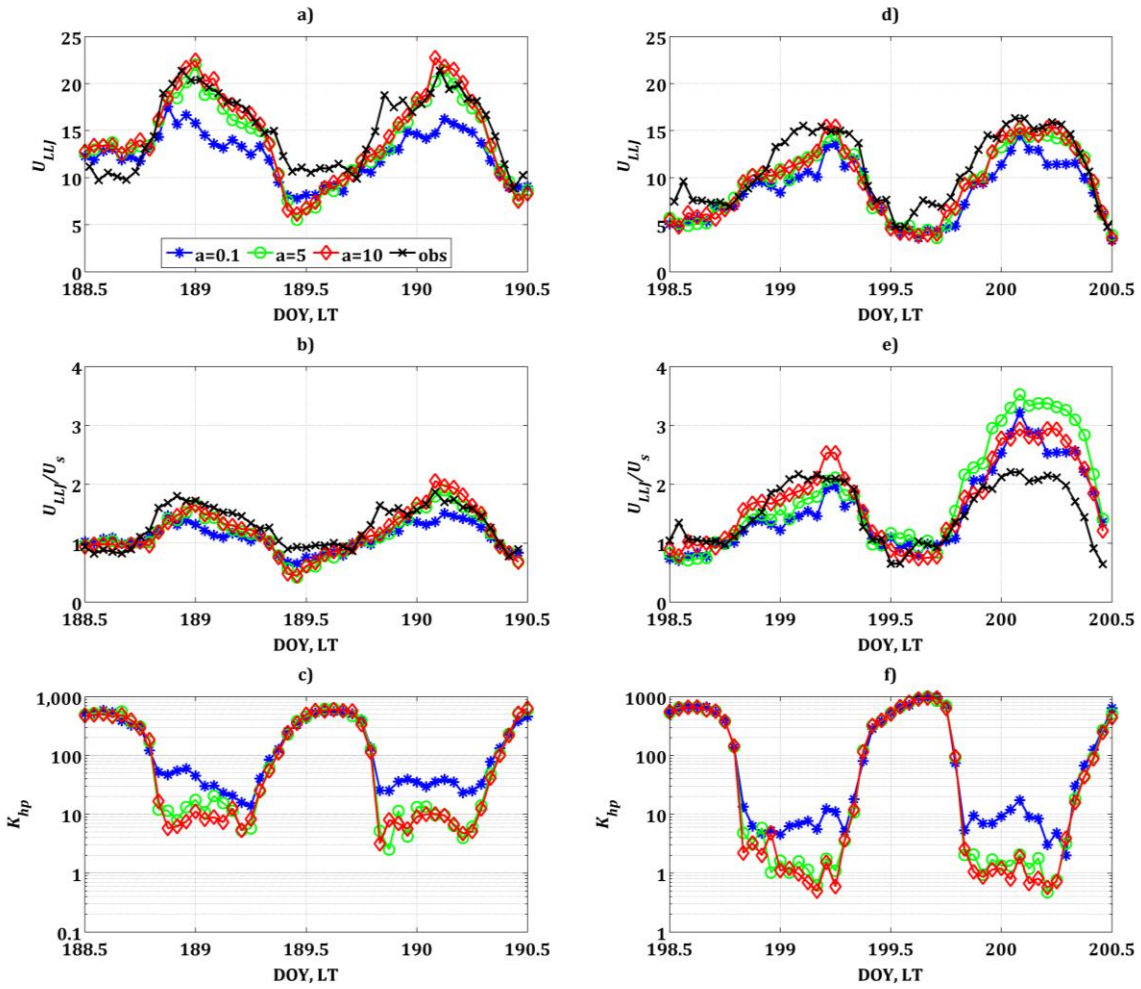

Figure 11. Time series of (a,d) maximum wind speed U_{LLJ}, (b,e) relative LLJ strength U_{LLJ}/U_s and (c,f) peak value of the eddy diffusivity K_{hp} in the boundary layer during the periods of (a-c) July 7-9 (DOY 188-190) and (d-f) July 17-19, 2003 (DOY 198-200). Results from WRF model sensitivity tests with the default YSU PBL scheme and three different values of the coefficient a in Eq. (5) are compared against the observations (obs).

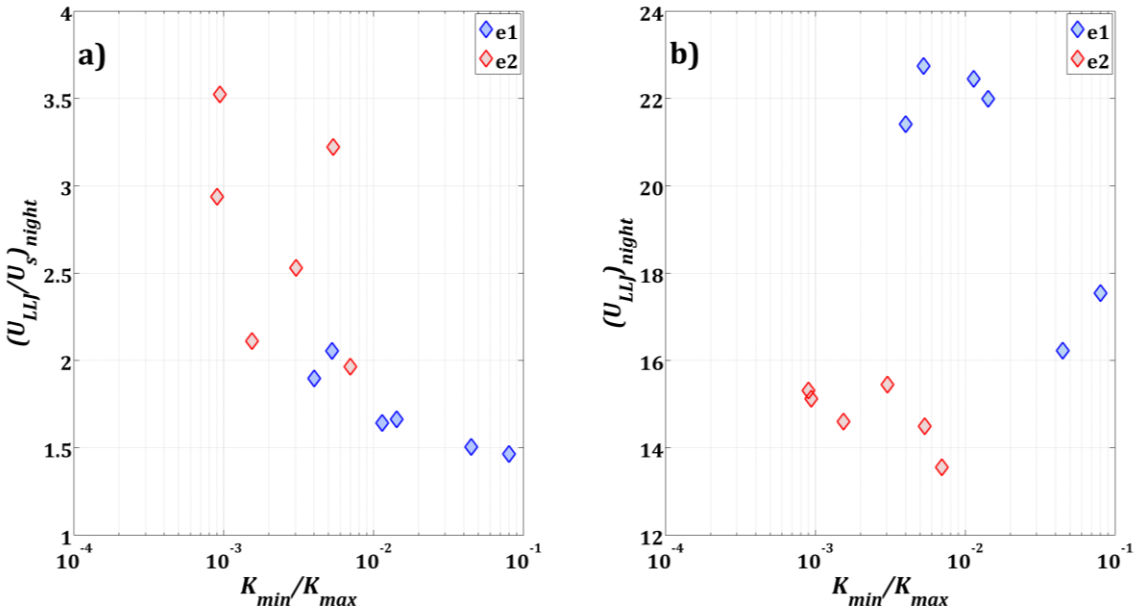

Figure 12. Variation of (a) relative LLJ strength $(U_{LLJ}/U_s)_{night}$ and (b) maximum wind speed $(U_{LLJ})_{night}$ with the ratio of nighttime to daytime eddy diffusivity K_{min}/K_{max}. The data plotted are based on the WRF model results shown in Fig. 11.

Revised-Figure 1 as png

Click here to download Figure: Fig1_revised_version.png

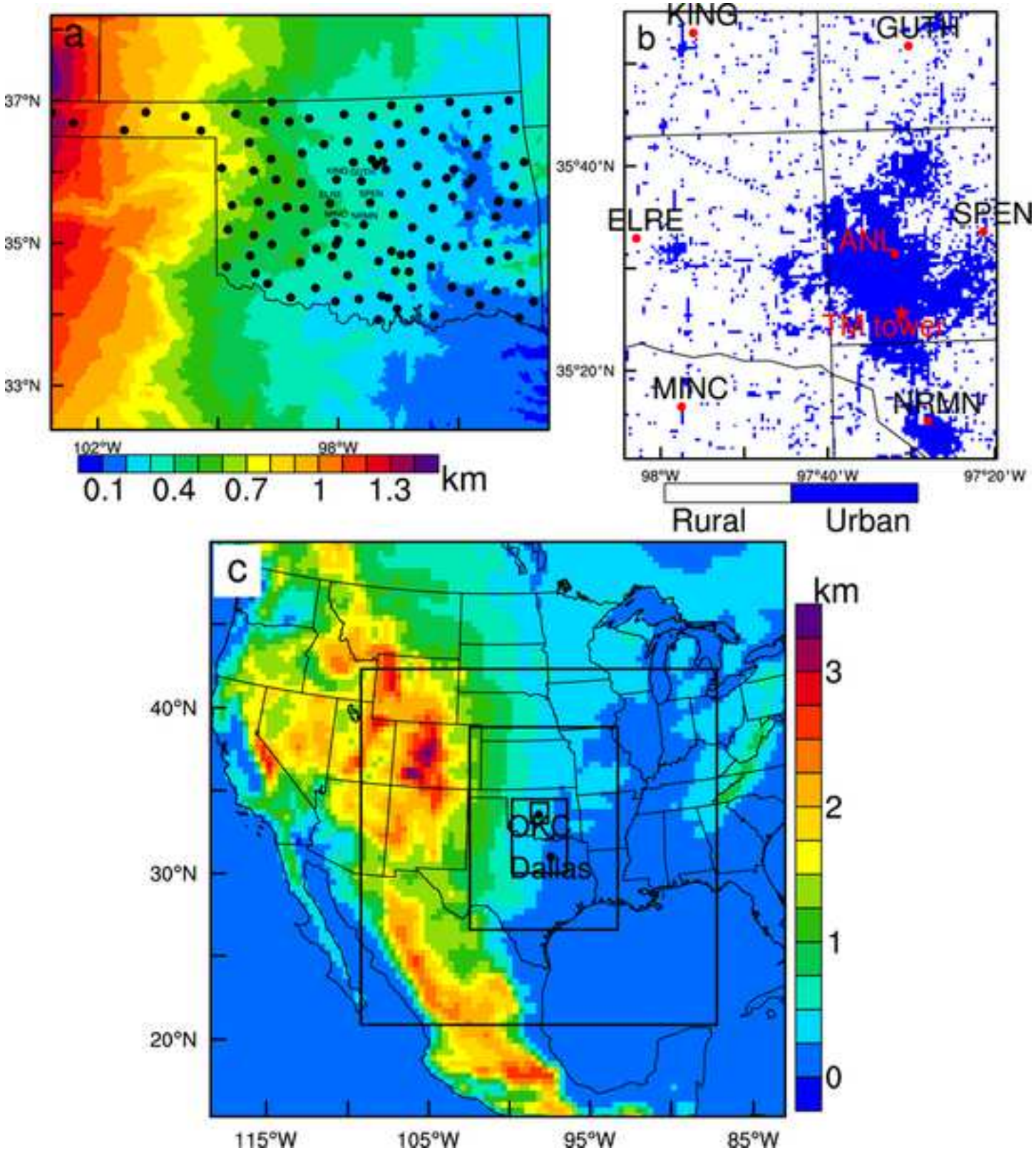

Revised Figure 2 as png
Click here to download Figure: Fig2_revised_version.png

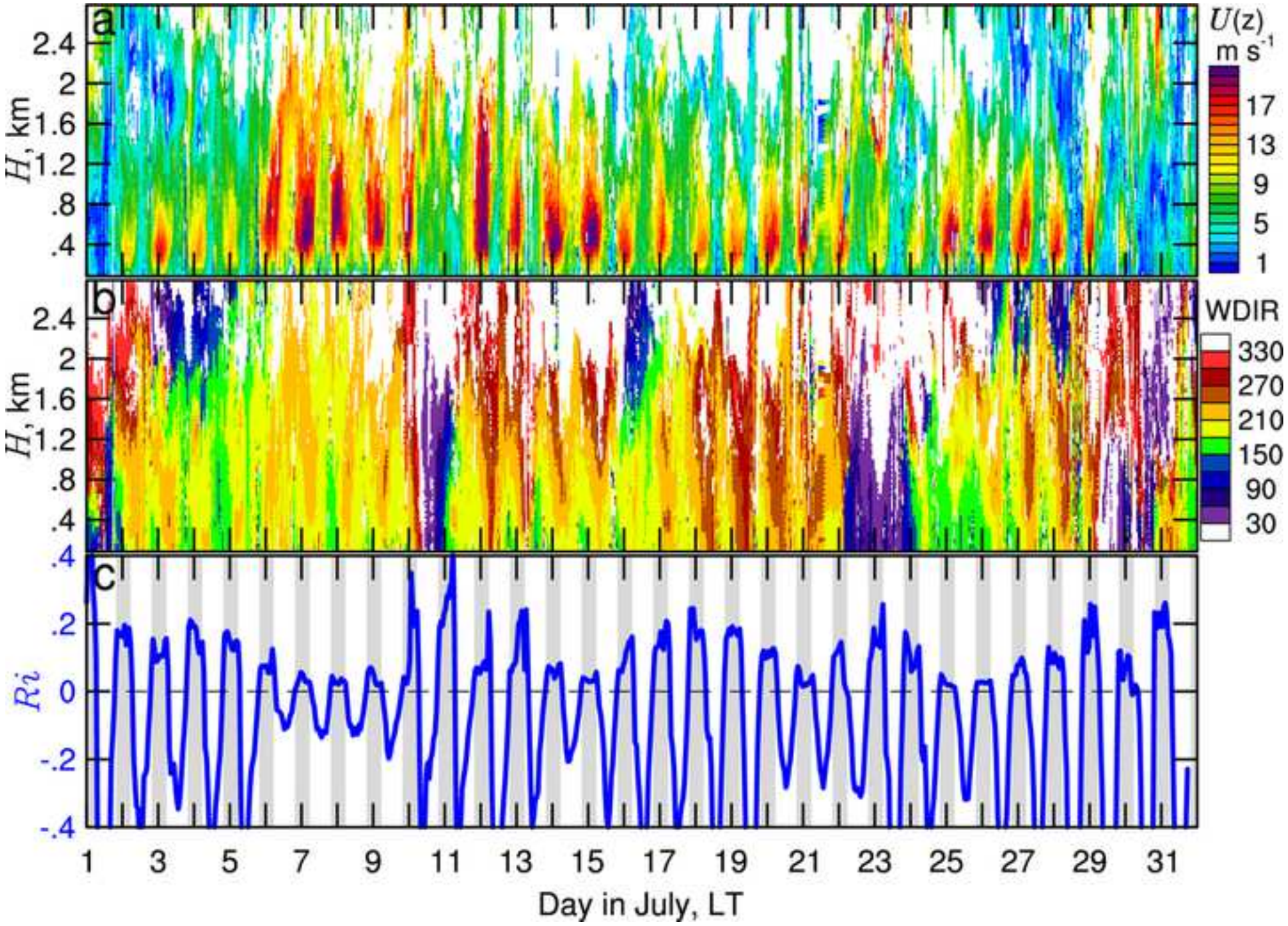

Figure 3 as png
Click here to download Figure: Fig.3_fv2.png

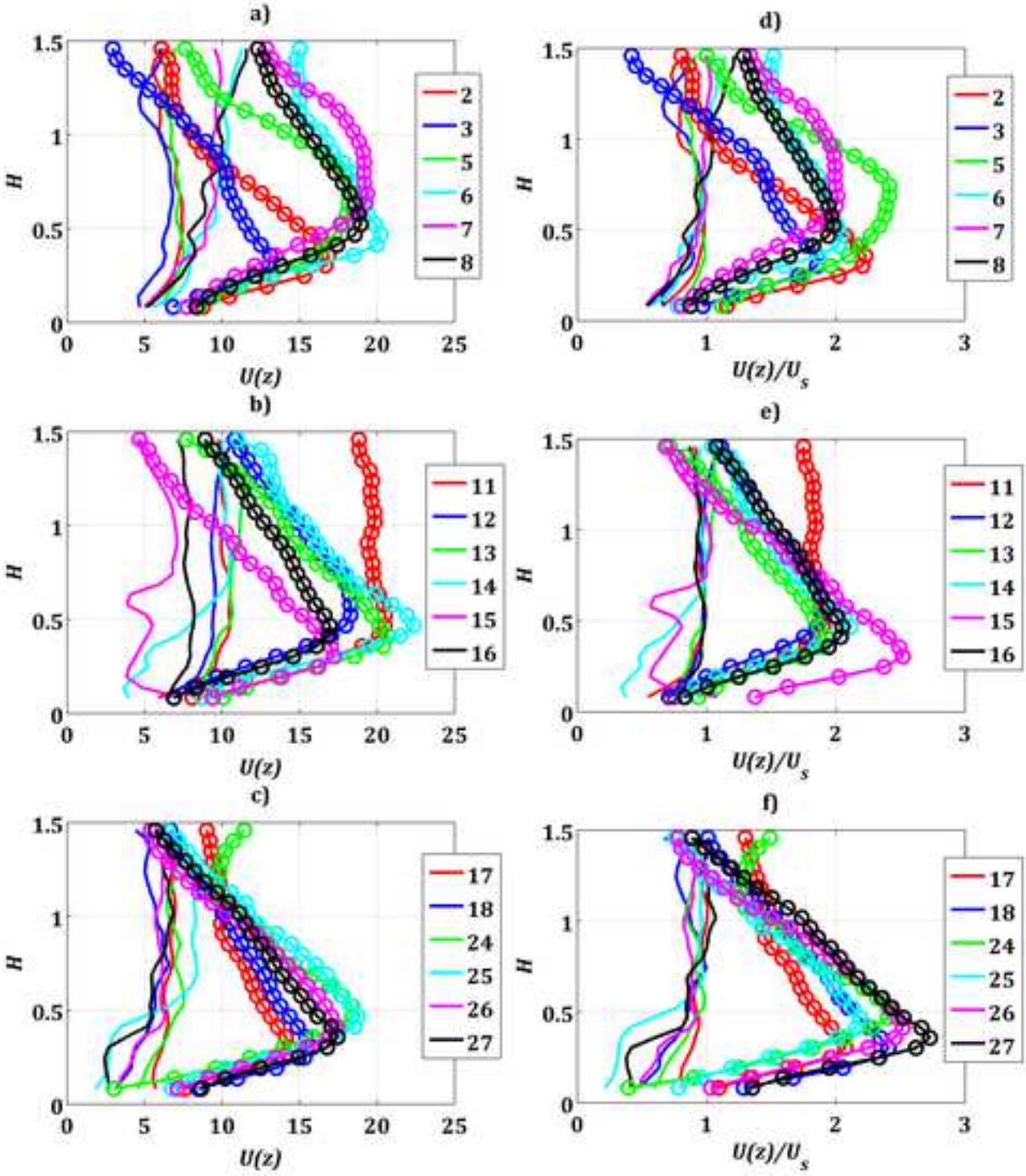

Revised Figure 4 as png

Click here to download Figure: Fig.4_rev.png

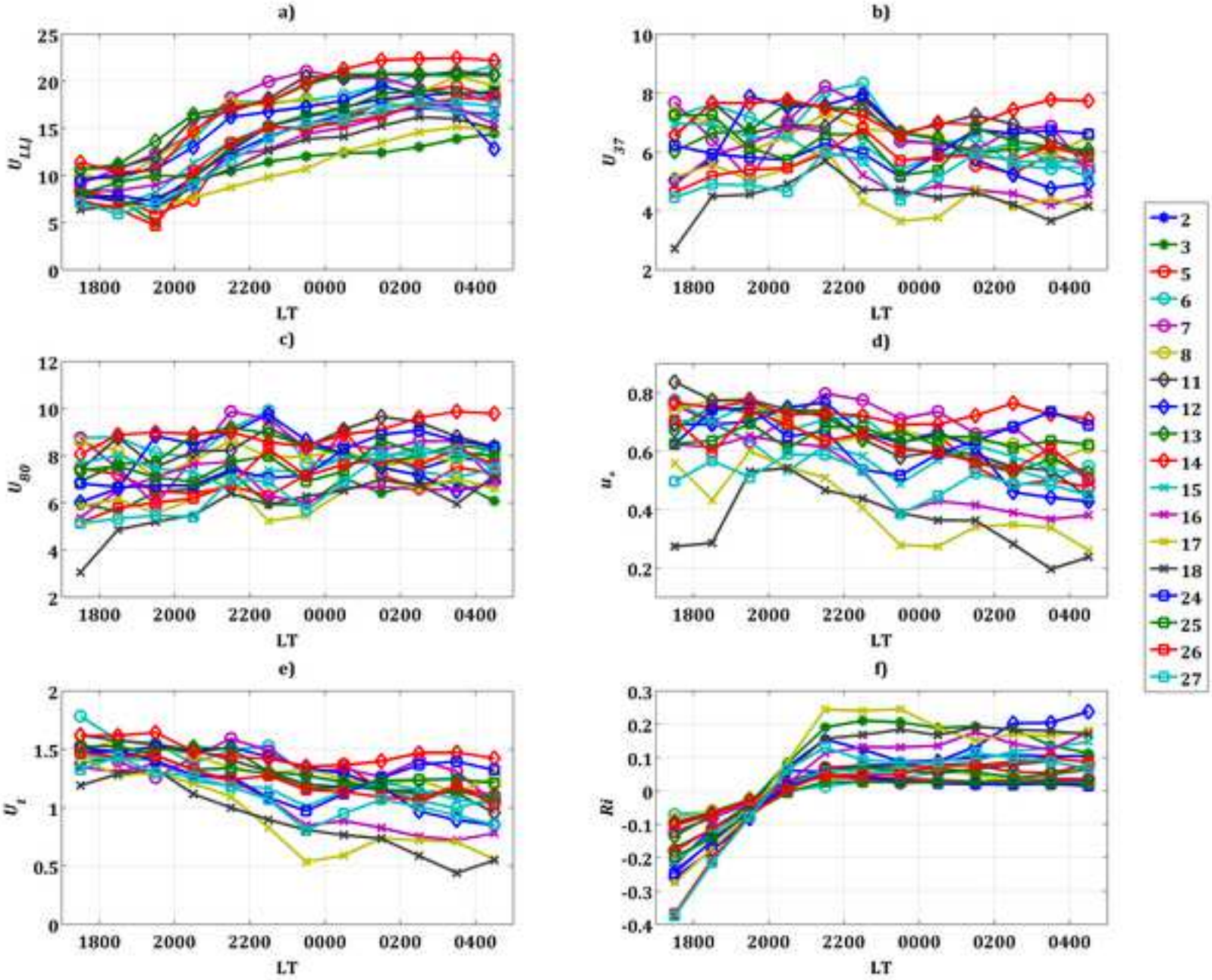

Revised Figure 5 as png

Click here to download Figure: Fig.5_rev.png

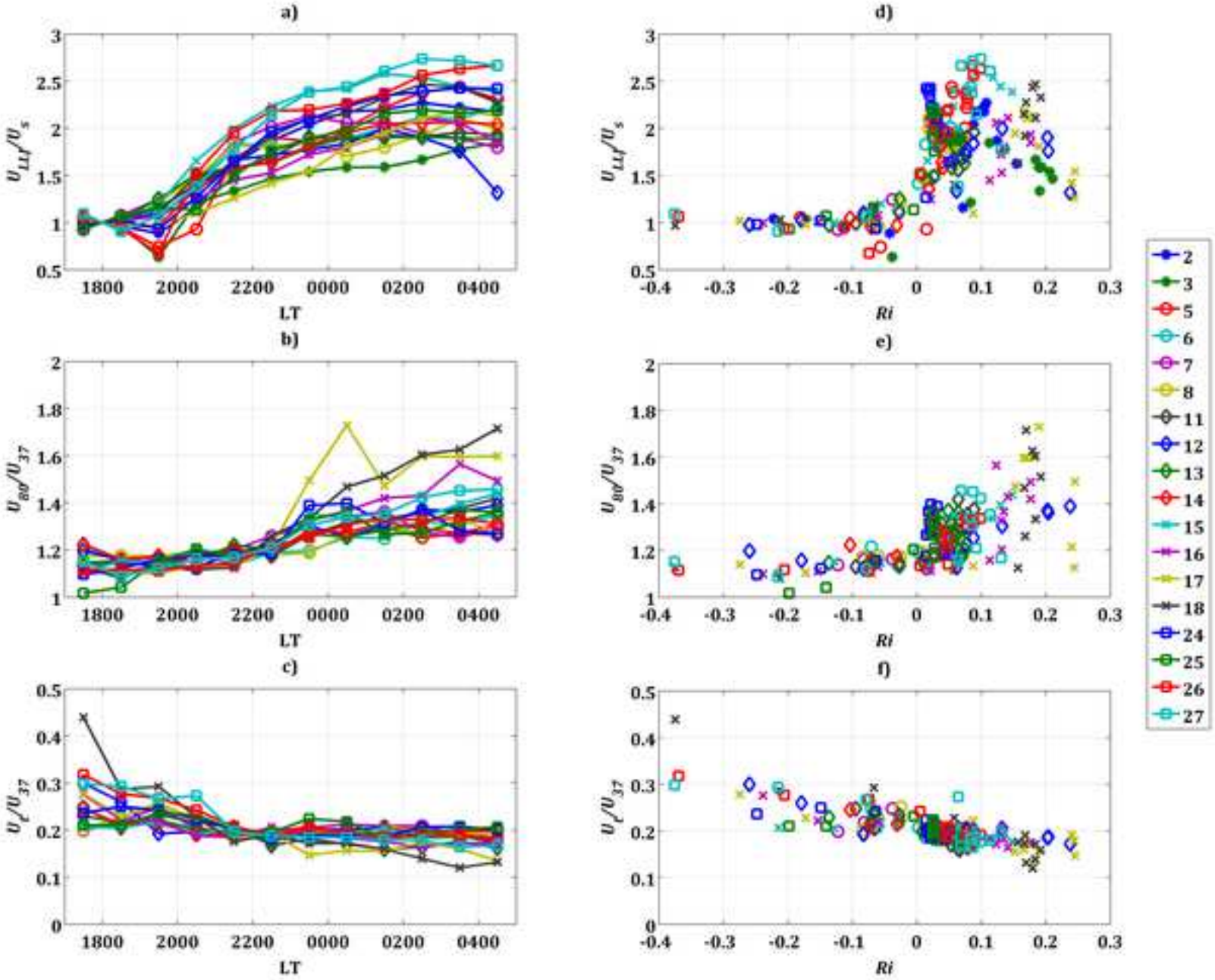

Figure 6 as png

Click here to download Figure: Fig.6_fv2.png

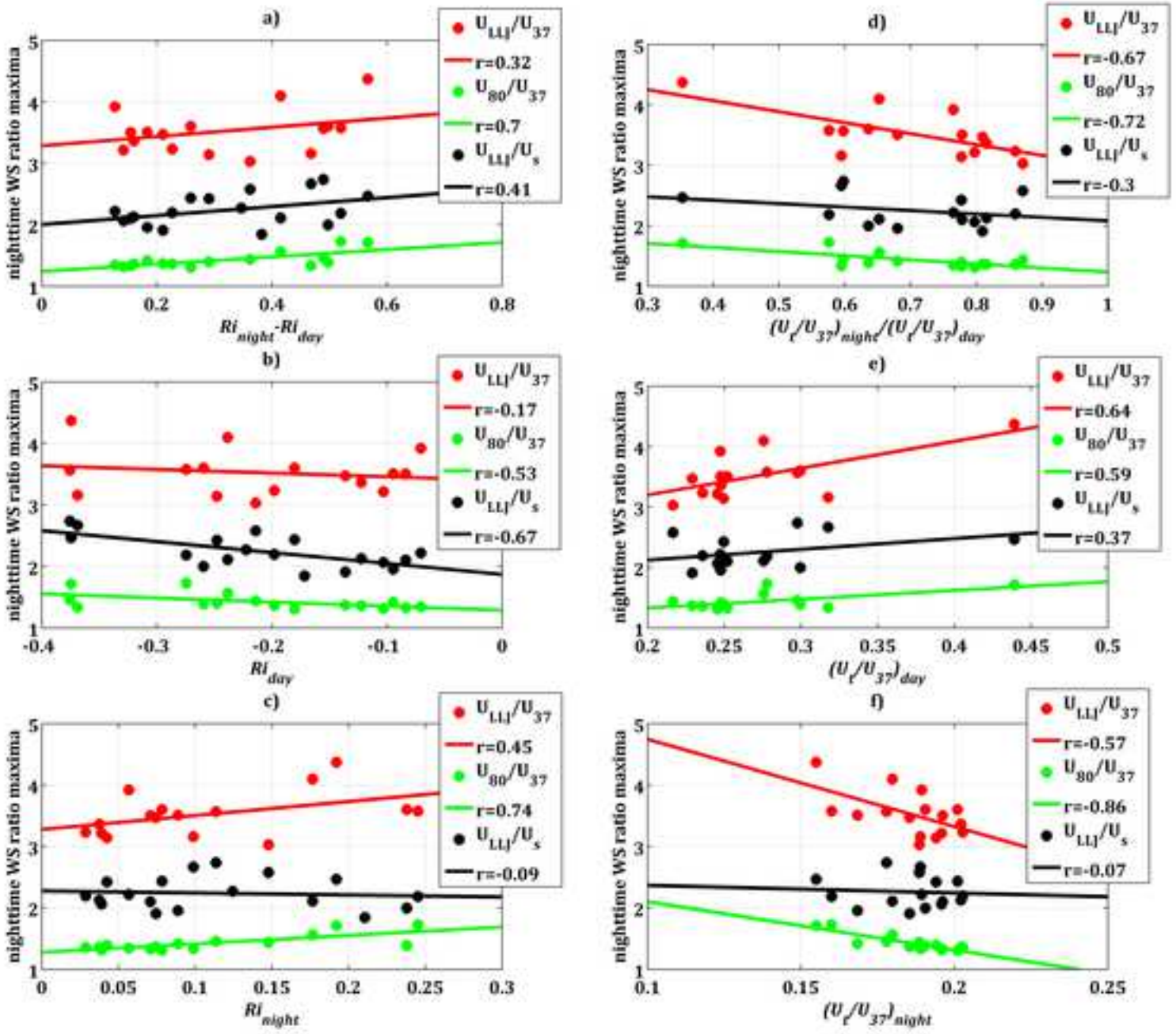

Figure 7 as png
Click here to download Figure: Fig.7_fv2.png

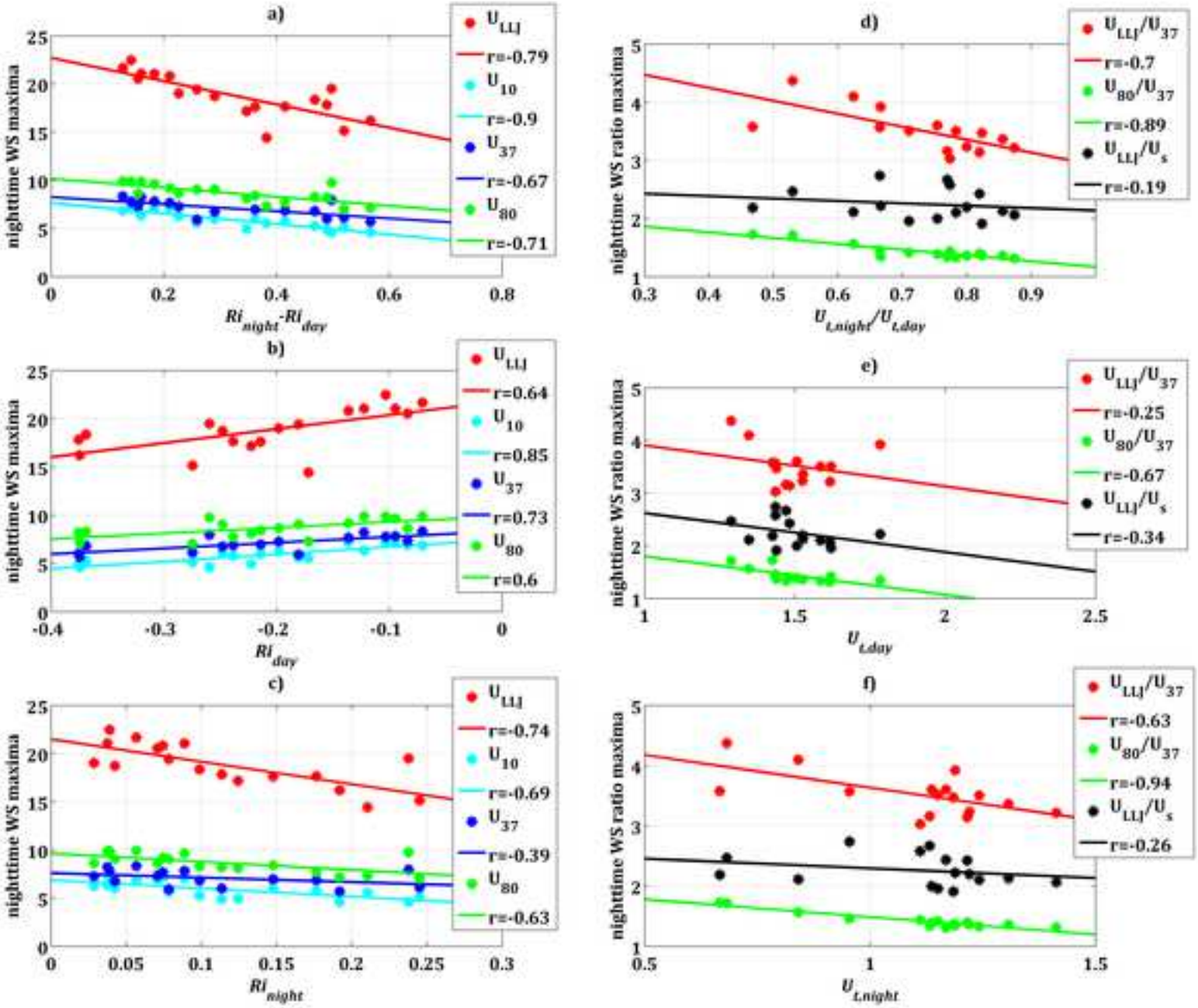

Revised Figure 8 as png
Click here to download Figure: Fig8_revised_version.png

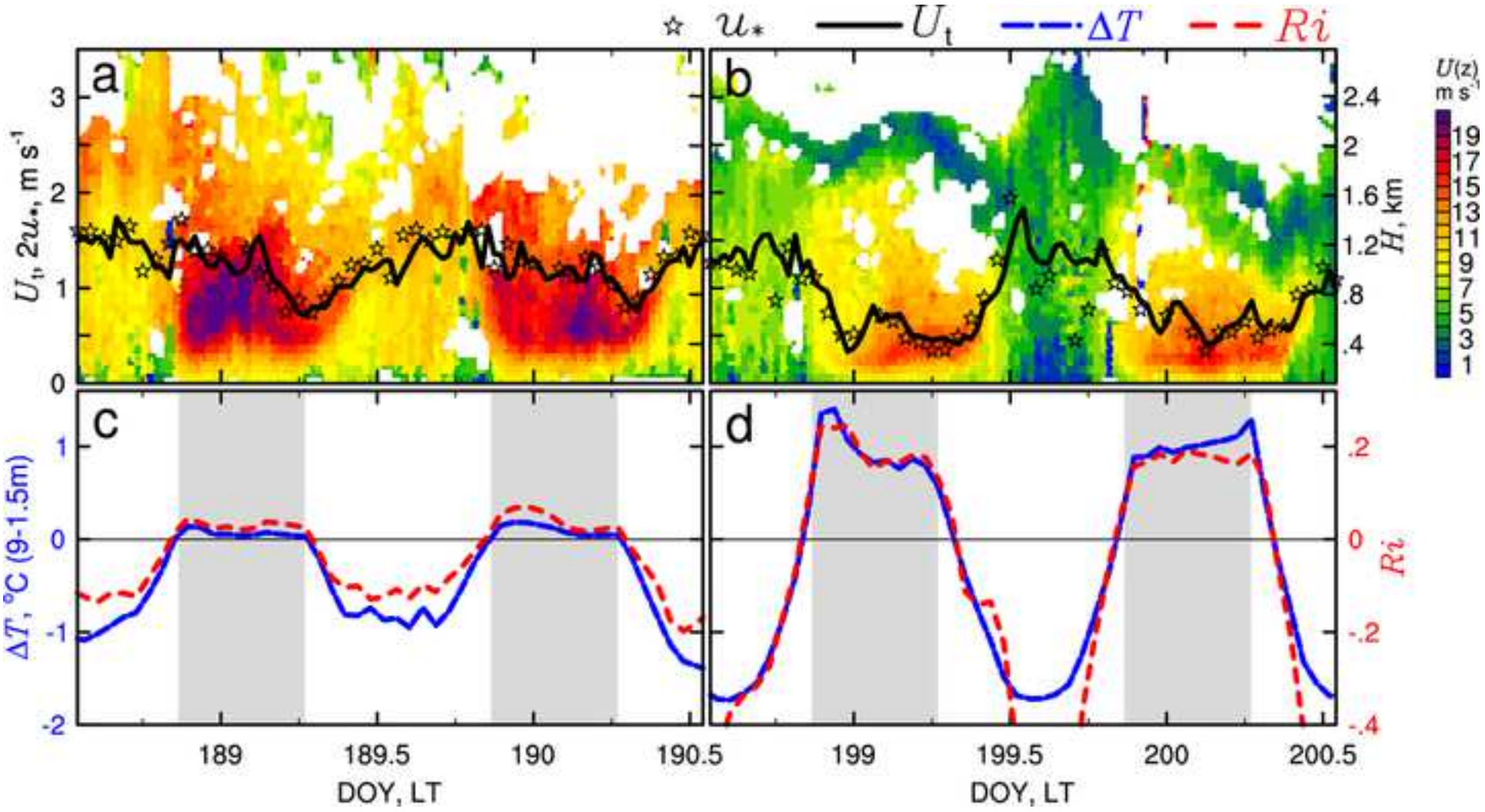

Revised Figure 9 as png
Click here to download Figure: Fig9_revised_version.png

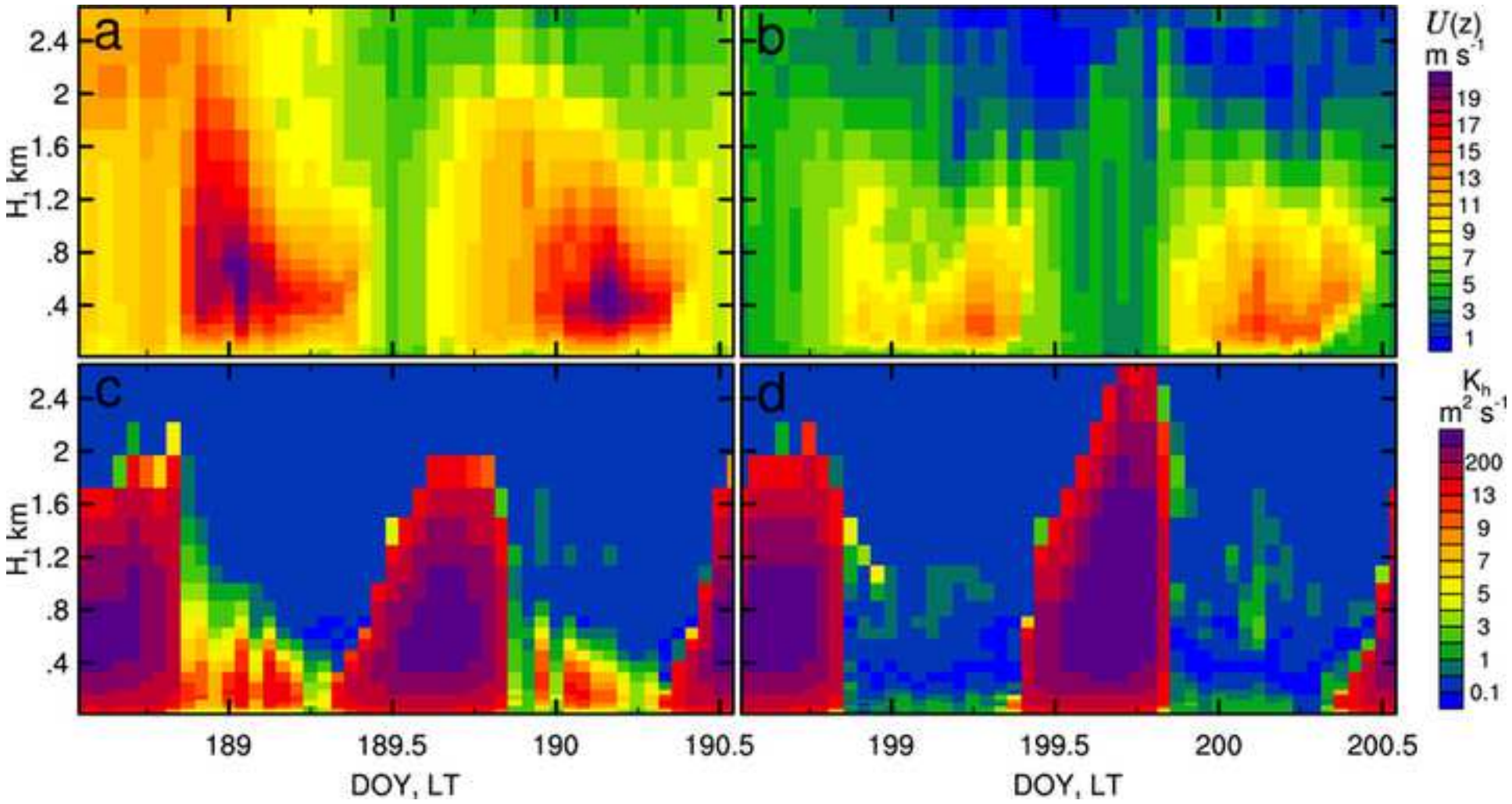

Revised Figure 10 as png

Click here to download Figure: Fig10_revised_version.png

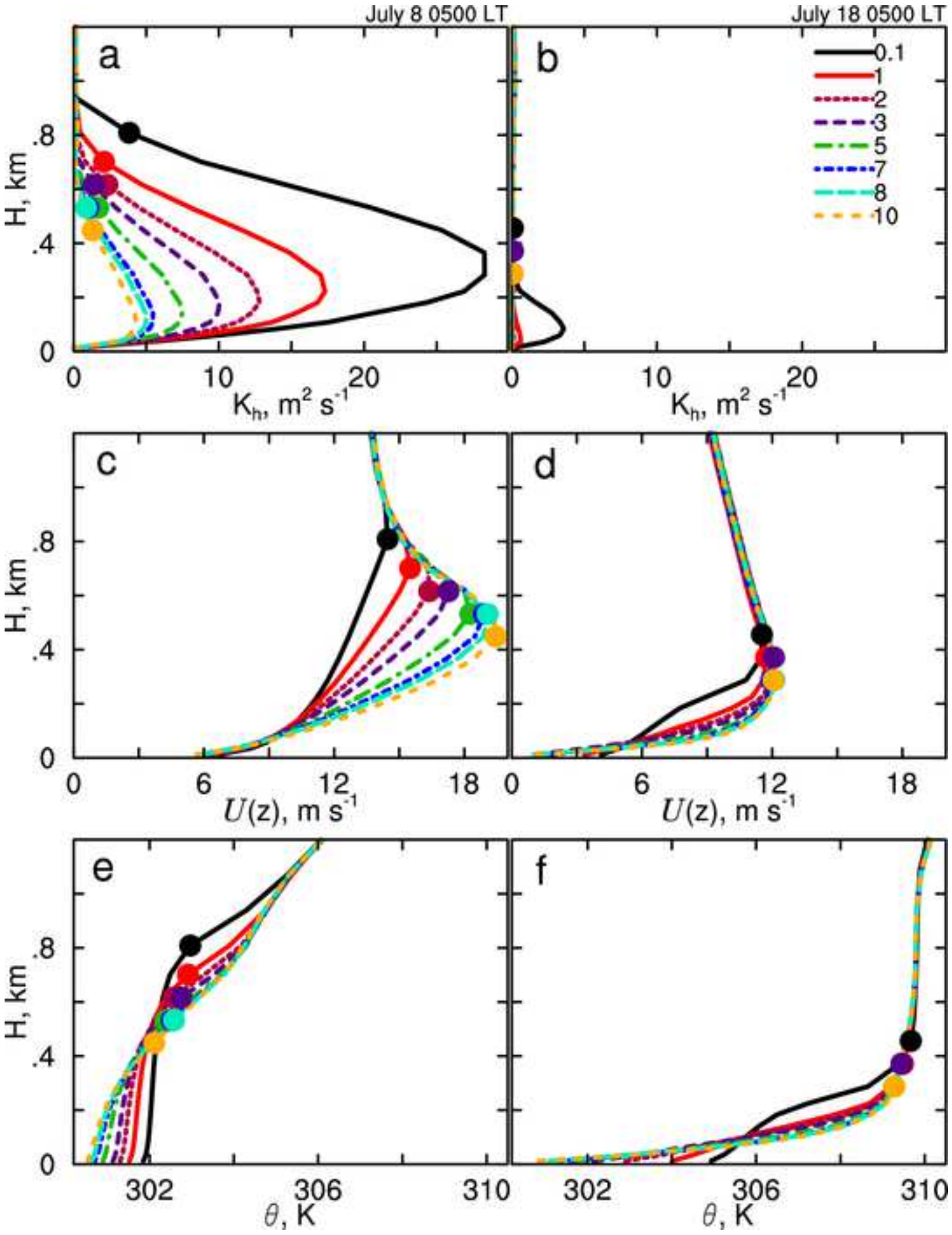

Figure 11 as png
Click here to download Figure: Fig.11_fv2.png

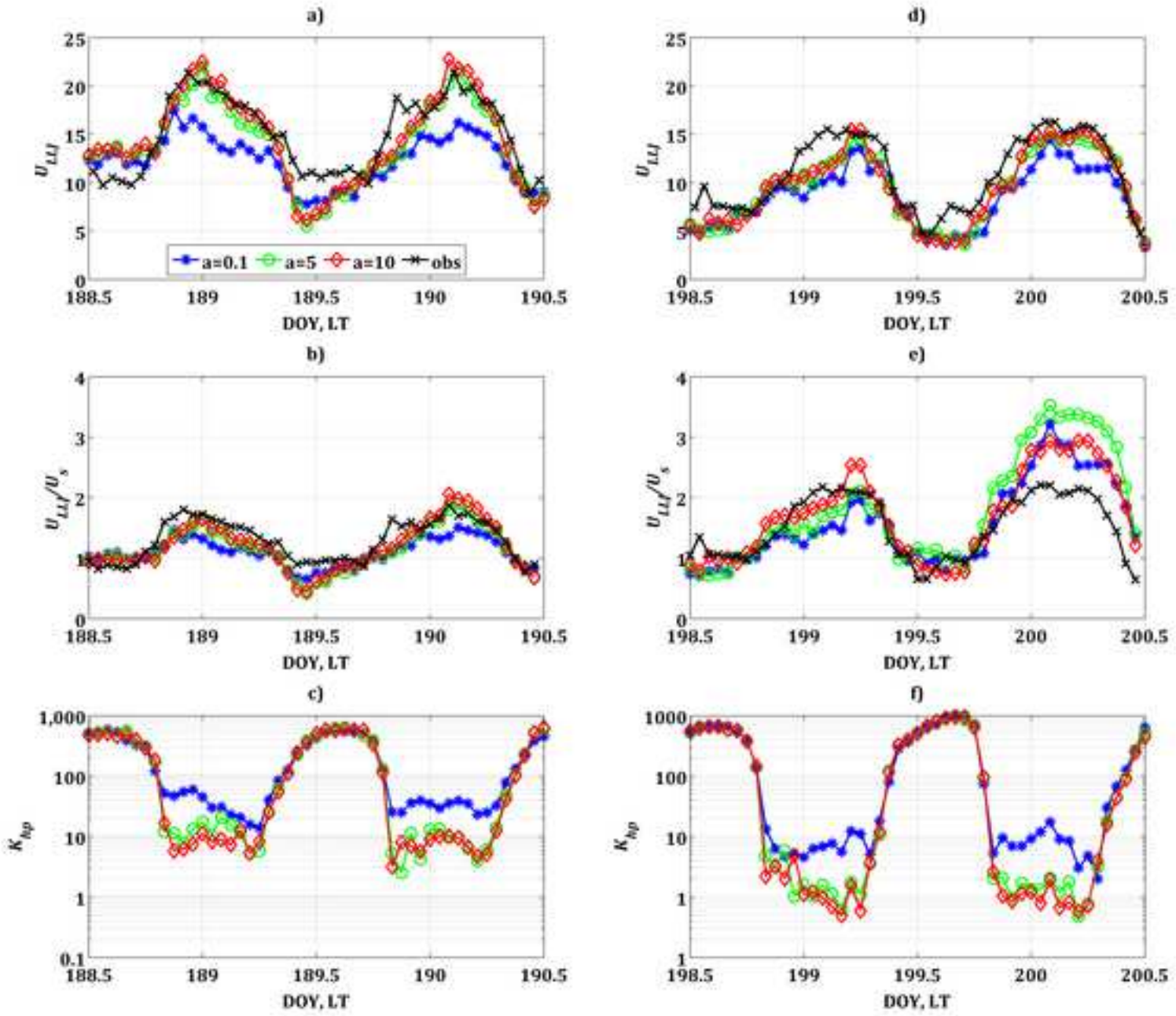

Figure 12 as png
Click here to download Figure: Fig12_fv.png